Rita Brekke

The role of lysine-specific demethylase 1A (LSD1) in Wnt driven cancer

December 2021

Master's thesis

Master's thesis 2021 Rita Brekke

NTNU
Norwegian University of Science and Technology
Faculty of Medicine and Health Sciences
Department of Clinical and Molecular Medicine

NTNU
Norwegian University of Science and Technology

NTNU
Norwegian University of Science and Technology

NTNU
Norwegian University of
Science and Technology

The role of lysine-specific demethylase 1A (LSD1) in Wnt driven cancer

Rita Brekke

Molecular Medicine
Submission date: December 2021
Supervisor: Menno Oudhoff
Co-supervisor: Mara Martin Alonso

Norwegian University of Science and Technology
Department of Clinical and Molecular Medicine

Abstract

Lysine specific demethylase 1A (LSD1) is an epigenetic modifier which interacts with various substrates and has diverse functions. Epigenetic dysregulation is emerging as a hallmark of cancer and thus, epigenetic inhibitors are a therapeutic target of interest. Earlier studies of organoid models show that LSD1 knockout (KO) organoids can grow in the absence of a WNT epithelial source (Paneth cells). In addition, LSD1 inhibition of intestinal organoids led to the expansion of the stem cell population. We demonstrate that LSD1 inhibition in a WNT driven organoid tumor model leads to morphological changes, namely an ellipsoid appearance as opposed to the spherical tumor organoid. We investigated the possibility that these change in morphology was related to changes in the cytoskeletal structure and we observed an increased expression of the actin binding protein Filamin A (FLNA) on LSD1 inhibition. A trend towards an increase in the expression of the WNT signalling pathway signal transducer protein β-catenin was observed. Another trend identified was an increase in the expression of the cell adherens junction protein E-cadherin which also displayed a cytoplasmic distribution as opposed to the predominantly membranal distribution seen in healthy intestinal epithelial cells. Whether the changes in morphology, WNT signalling pathway factors and cytoskeletal proteins are indicative of a reduction or an increase in characteristics favourable to tumor survival requires further *in vivo* studies.

Acknowledgements

This thesis was conducted at the Centre of Molecular Inflammation Research (CEMIR), a department under the Faculty of Medicine and Health Sciences, Norwegian University of Science and Technology (NTNU), Trondheim.

I would like to thank my principle supervisor Menno Johannes Oudhoff for his big picture guidance, encouragement and being very understanding when I have had a difficult year with my health during the course of this thesis. Mara Martin Alonso, thank you for being an incredibly good teacher and guiding me through the techniques used. I have learnt an incredible amount from you and I am extremely appreciative of your patience, encouragement and support.

Kjartan Wøllo Egeberg and Bjørnar Sporsheim thank you for training and guiding me through the imaging techniques used in this thesis.

I have benefited greatly from many members of the research group and would like to thank Alberto Diez Sanchez, Naveen Parmar and Pia Vornewald for answering my many questions, always being approachable and giving me help when I needed it.

On a personal note, I have been very lucky to have friends and family who have been very supportive. Thank you Tommy Ingemar Steen for providing me with a lovely work space, incredible amounts of emotional support and a strong belief in my abilities. I have to thank my two little boys, Storm and Sverre Brekke for being patient and understanding when I have been busy. I am greatly appreciative of Edmund Førland Brekke for taking on a larger share of the parenting load while I pursued this.

Table of Contents

List of Figures

Abbreviations

APC	Adenomatous polyposis coli
BCA	Bicinchoninic acid
BMI1	B lymphoma Mo-MLV insertion region 1 homolog
BMP	Bone morphogenetic protein
BSA	Bovine serum albumin
CBC	Crypt base columnar cell
CDX2	Parahox gene caudal type homeobox protein 2
CoREST	REST corepressor 1
CRE-ERT2	Cre recombinase fused to a mutant estrogen receptor
CRC	Colorectal cancer
CSC	Cancer stem cell
DKK1	Dickkopf1
EGF	Epidermal growth factor
EGFP	Enhanced green fluorescent protein
EMT	Epithelium-to-mesenchyme transition
FAP	Familial adenomatous polyposis
FLNA	Filamin A
GSK-LSD1	Selective inhibitor of LSD1
H3K4/9	Histone 3 lysine 4/9
HOPX	Homeodomain-only protein homeobox
IF	Immunofluorescence
ISC	Intestinal stem cell
IWP-2	WNT inhibitor
KO	Knockout
KRAS	Kirsten rat sarcoma viral oncogene
LGR5	Leucine-rich-repeat-containing G protein coupled receptor
LOXP	Locus of X over P1
LRIG1	Leucine rich repeats and immunoglobulin-like domains protein 1
LRP5/6	Lipoprotein receptor related protein 5
LncRNA	Long non-coding RNA
LSD1	Lysine specific demethylase 1A
me1/me2	Mono-/dimethyl

MUC2	Mucin 2
NGS	Normal goat serum
OLFM4	Olfactomedin 4
ORY-1001	Selective inhibitor of LSD1
PBS	Phosphate buffered saline
PFA	Paraformaldehyde
RNF43	RING finger protein 43
RSPO	R-spondins
SLUG	Snail family transcriptional repressor 2
SMAD	Small mothers against decapentaplegic
SNAIL	Snail family transcriptional repressor 1
SOX9	SOX9
SWIRM	Swi3/Rsc8/Moira domain
TA	Transit amplifying
TBST	Tris buffered saline and tween
TCF	T cell factors
TERT	Telomerase reverse transcriptase
TGF	Transforming growth factor
TNM	Tumor node metastasis
UEA1	Ulex europaeus agglutinin-1
WNT	Wingless-related integration site
WT	Wild type
ZNRF3	Zinc/RING finger protein 3

1 Introduction

1.1 The intestinal tract.

The gastrointestinal tract is a single muscular tube that stretches from the oral cavity to the anus. The gastrointestinal tract, with exception of the esophagus is spanned by a single layer of cells that forms the epithelium. The intestinal tract has a surface area of about $30m^2$ in humans, which makes it the second largest epithelial system in the body (Helander & Fändriks, 2014). The intestinal epithelium is unique in having to carry out various opposing roles; it has the task of absorption, while simultaneously it is subject to various harsh luminal insults such as pathogens and antigens and must act as an effective barrier. The intestinal epithelium must fulfill a multipurpose role and the way tissue is organized is key to achieving this.

The intestine is organized into a mucosal and a submucosal layer (figure 1-1). The main functions of the mucosal layer are absorption of dietary nutrients and water, secretion of digestive enzymes and protection against microbes and noxious substances. The mucosal layer can be divided into 3 layers starting from the lumen consisting of epithelium, the lamina propria and the muscularis mucosa. The epithelium is organized into multiple crypt-villus units that project into the lumen. Below the epithelium lies the lamina propria; a connective tissue where immune cells, mesenchymal cells, endothelial cells, and nerve cells reside. The muscularis mucosae consist of a thin layer of smooth muscle cells.

The submucosa is a dense connective tissue layer, beyond which two thick smooth muscle layers: the inner 'circular' and outer 'longitudinal', form the muscularis externa. The muscularis externa is responsible for segmentation and peristaltic movements. In addition, nerve plexuses are found in the submucosal layer and between the longitudinal and circular layers of the muscularis externa.

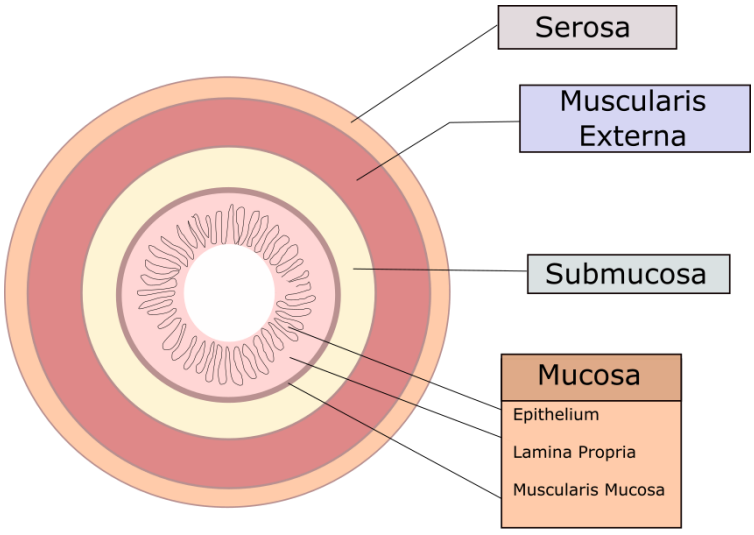

Figure 1-1: Layers of the small intestine. Illustration made in Inkscape.

1.2 The intestinal crypt-villus structure

The crypt-villus unit is composed of one finger like protrusion into the lumen surrounded by multiple invaginations called crypts. Millions of these crypt-villus units are organized to form the intestinal epithelium (Gehart & Clevers, 2019). The villus in the small intestine is covered by postmitotic epithelium which mediates nutrient uptake and serves as a barrier. Absorbed nutrients are made immediately accessible to the liver and the rest of the body by a dense network of capillaries and lymph vessels. Villi length varies along the intestine, going from about 1mm in the duodenum to being completely absent in the colon. The surface area is significantly increased due to the folding of the intestinal epithelium in the form of protrusions into the lumen. This in combination with the excellent accessibility to the circulatory system greatly improves the absorptive capability of the intestine.

The epithelial layer is exposed to the environment of the lumen as well as mechanical stress. The overall lifetime of the intestinal epithelial cells is about 3 to 5 days. The quick turnover reduces exposure of the epithelium to potential damage (Darwich et al., 2014). The crypt is protected from the harsh luminal environment due to its recessed position as well as the mucus layer that coats the intestinal epithelium. As shown in figure 1-2, at the base of the crypt are continuously dividing stem cells that give rise to progenitor cells in what is known as the transit amplifying zone. The cells in the transit amplifying (TA) zone rapidly proliferate and become mature intestinal epithelial cells. Hence, cells make a trip from the base of the crypt towards the tip of the villus as they are pushed by the following generation of epithelial cells. Here, they eventually are shed into the lumen and undergo anoikis. This ingenious arrangement allows the more vulnerable actively proliferating cells to be sheltered while only postmitotic cells are exposed to the hazardous luminal contents for a short time. Furthermore, this mechanism protects from cancer, as mutations that arise in cells due to the hazardous luminal contents will not drive tumour formation for, they are sloughed off before this can occur.

The epithelium is divided into absorptive and secretory lineages. Enterocytes are absorptive, and Paneth, goblet, enteroendocrine and tuft cells makes up the secretory lineage. The different cells have specialized functions essential to smooth functioning of the intestinal tract. Hence, a continuous supply of all cell types in the right proportions is necessary and hence the role of the intestinal stem cell is pivotal.

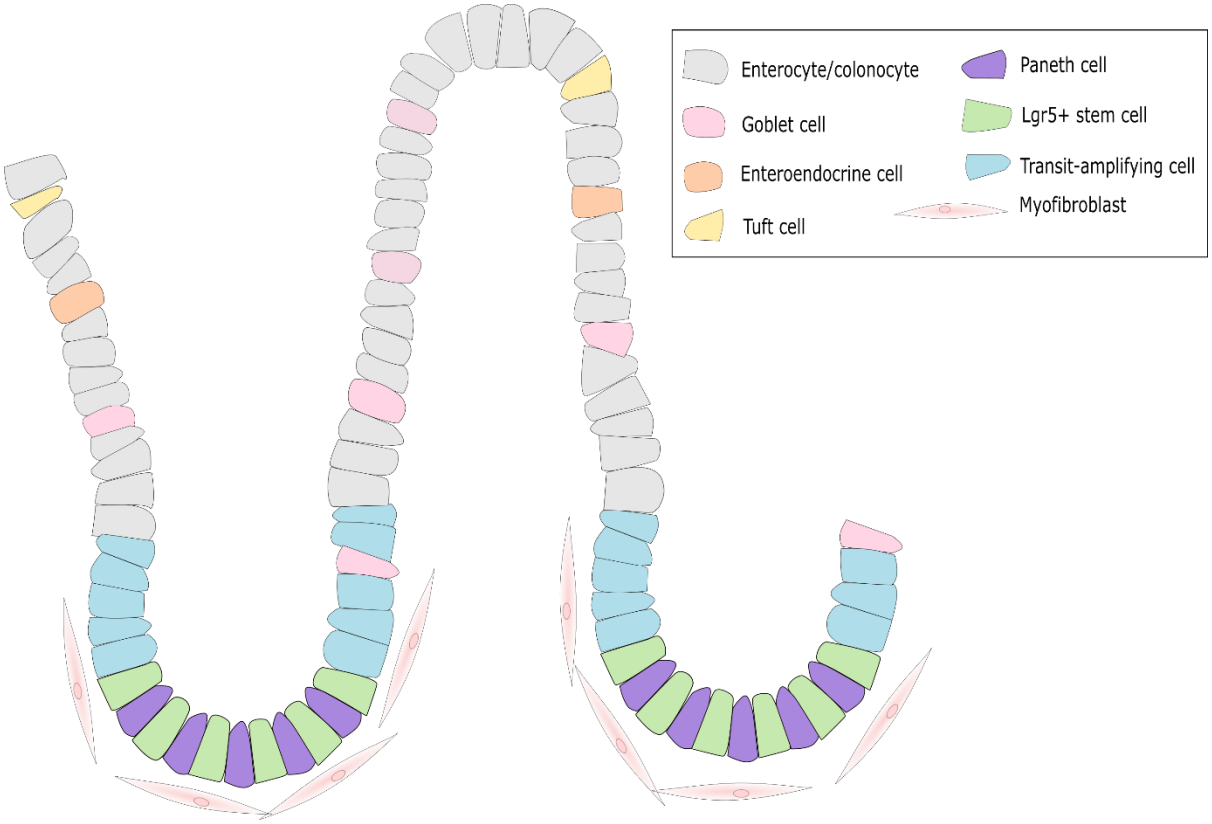

Figure 1-2: Organization of a crypt-villus unit. Illustrated in Inkscape

1.2.1 The intestinal stem cell

An intestinal stem cell (ISC) is a cell capable of continuous self-renewal by dividing into daughter cells or progenitor cells that differentiate into the various mature epithelial cell types. The crypt base columnar cell (CBC) was identified as a potential stem cell by Cheng and Leblond when they showed that CBCs were continuously cycling cells that acted as a common source for the other epithelial lineages(Cheng & Leblond, 1974). These CBCs exclusively express a WNT target gene, leucine -rich-repeat-containing G-protein-coupled receptor 5 (LGR5). Lineage tracing experiments confirm the identity of these $LGR5^{+}$ CBCs as stem cells by demonstrating that all epithelial lineages were generated from these, and furthermore that they were capable of self-renewal (Barker et al., 2007). In addition, to LGR5 expression as a marker of these stem cells, olfactomedin 4 (OLFM4) has also been identified as a robust marker (van der Flier et al., 2009).

It has been postulated that a population of reserve stem cells separate from the above mentioned CBCs exist. Chris Potten identified the +4 cells as another population of stem cells (Potten, 1977). The +4 cell is named such as it is positioned in the +4 location just above the uppermost Paneth cell. Specific genetic markers of +4 cells such as B lymphoma Mo-MLV insertion region 1 homolog (*Bmi1)*, telomerase reverse transcriptase (*Tert)*, homeodomain-only protein homeobox (*Hopx)* and leucine rich repeats and immunoglobulin-like domains protein 1 (*Lrig1)* have been identified (Breault et al., 2008; Montgomery et al., 2011; Sangiorgi & Capecchi, 2008; Takeda et al., 2011; Y. Wang et

al., 2013). This population of ISC is resistant to injury and genetic lineage tracing experiments shows that they replenish the intestinal epithelium and CBC cells (Breault et al., 2008; Montgomery et al., 2011; Sangiorgi & Capecchi, 2008; Takeda et al., 2011; Y. Wang et al., 2013; Yan et al., 2012). However, the expression of +4 markers was detected in CBC cell lines as well and may not be specific to the +4 stem cells, and so there is debate regarding the presence of a distinct population of quiescent reserve stem cells (Grün et al., 2015; Muñoz et al., 2012; F. Wang et al., 2013; Wong et al., 2012). The expression of these markers in other cell populations does not negate the possibility of a distinct +4 stem cell population. However, the possibility that several cell types in the TA zone may revert to stem cells upon damage has been shown indicating a more plastic model of regeneration might be considered (Cheng & Leblond, 1974; Marshman et al., 2002).

1.2.2 The intestinal stem cell niche

ISCs depend on the surrounding microenvironment for necessary factors, and this is known as the intestinal stem cell niche. Various cells have been identified as important for maintaining this niche; myofibroblasts producing wingless-related integration site (WNT) agonists and bone morphogenetic protein (BMP) antagonists (Lei et al., 2014), smooth muscle cells produce BMP antagonists (Kosinski et al., 2007), endothelial cells produce fibroblast growth factor, Paneth cells produce WNT ligands, Notch ligands, epidermal growth factor (EGF) and transforming growth factor α (TGF-α) (Sato, van Es, et al., 2011). These are necessary for ISCs to retain their stemness and so every ISC is in contact with at least one Paneth cell. Regenerating family member 4 positive staining deep secretory cells potentially fulfil the same role in the colon, where Paneth cells are not found (Sasaki et al., 2016). In addition, Paneth cells produce lactate which is a substrate for mitochondrial metabolism in ISCs (Rodríguez-Colman et al., 2017).

1.3 Signalling pathways.

The proliferation and differentiation of intestinal epithelia is orchestrated by the interplay of a variety of pathways such as WNT, Notch, BMP, EGF.

1.3.1 WNT pathway

Stem cell maintenance is strongly linked to the WNT pathway. Disruptions in this pathway is associated with cancer development in the intestinal epithelium. β-catenin is an effector protein of the WNT pathway and has a key role. In the WNT inactive state, cytoplasmic β-catenin, is phosphorylated upon binding with the adenomatous polyposis coli (APC) destruction complex, which marks it for destruction by ubiquitylation. The 'destruction complex' consists of APC, glycogen synthase 3β, casein kinase 1 α and the scaffold protein axis inhibition protein 1. Upon WNT activation, WNT ligands bind to the Frizzled-Low-density lipoprotein receptor-related protein 5-6 (LRP5-LRP6) receptor complex which inactivates the APC destruction complex (Nusse & Clevers, 2017). Thus, β-catenin is not destroyed and accumulates in the cytoplasm. β-catenin is then translocated to the nucleus where it binds T cell factors (TCFs) to form a transcription complex which regulates gene expression.

R-spondins are a family of four distinct secreted proteins (RSPO1, RSPO2, RSPO3 and RSPO4) which act as potentiators of WNT signalling and is necessary for intestinal stem cell maintenance (De Lau et al., 2014; Kim et al., 2006). RSPO2 has been found to be secreted by cells in the sub-epithelial stromal compartment (Kang et al., 2016). R-spondin binds to receptors of the LGR family, such as LGR5 the ISC marker, which in turn recruits RING finger protein 43 (RNF43) or Zinc/RING finger protein 3 (ZNRF3). RNF43 and ZNRF3 are transmembrane E3 ubiquitin ligases that binds and ubiquitinates the WNT receptor Frizzled, marking it for destruction. Thus, the amount of free RNF43 and ZNRF3 regulates the availability of Frizzled. When R-spondin activates the sequestering of free RNF43 and ZNRF3, the degradation of Frizzled receptors is blocked and hence WNT ligand sensitivity is increased (De Lau et al., 2014).

A gradient of WNT ligand concentration from the crypt base to villus occurs due to the low solubility of WNT ligands. WNT ligands are carried on the surface of cells and hence the gradient is dependent on the upward migration of differentiating cells from the crypt base. R-spondin also helps with the gradient by increasing surface availability of WNT ligands. R-spondin itself is highly soluble. The amount of surface WNT is halved with every cell division outside of the stem cell zone. This leads to a higher concentration in the crypt base and a lower concentration at the villus and forms a dynamic feedback loop where speed of proliferation is associated with WNT availability (Gehart & Clevers, 2019).When stem cell proliferation is rapid, cells will move quicker upwards in the crypt Rapid stem cell proliferation will lead to many cells moving upwards in the crypt causing the WNT gradient to be drawn out. Thus, there will be lowered WNT availability in the stem cell zone, which in turn slows down proliferation of ISCs. The reverse is also true where a reduction in proliferation due to damage of the stem cell population causes the gradient to shorten and positive feedback is established supporting stem cell proliferation and de-differentiation of progenitor cells (Gehart & Clevers, 2019).

WNT signalling is essential for intestinal stem cell development. This can be seen in studies of the downstream WNT effector TCF4. In an experiment of *Tcf4* knockout neonatal mice the complete loss of stem cells and breakdown of the epithelium was observed (Korinek et al., 1998). Another study involving the conditional deletion of *Tcf4* in adult mice resulted in the rapid loss of LGR5+ cells (Van Es et al., 2012). Similar results were demonstrated when Dickkopf1 (DKK1) a WNT inhibitor was overexpressed in adult mice (Kuhnert et al., 2004). Hence, the WNT signalling pathway is a key in the maintenance of stem cells.

On the flipside, excessive WNT signalling causes excessive intestinal epithelial growth. In human familial adenomatous polyposis (FAP) patients, the most common mutation is a deletion mutation in codon 1309, with the next most common being a deletion in codon 1061 of the *APC* gene. There are more than 300 mutations identified as a cause of FAP, which result in a truncated APC protein (Half et al., 2009). In mouse models, conditional deletion of *APC* in murine intestinal stem cells leads to large adenomas forming (Barker et al., 2009). In the heterozygous $Apc^{Min/+}$ mouse, a nonsense mutation at the *Apc* locus results in truncation of the APC protein leading to spontaneous adenomas similar to that in human FAP (Moser et al., 1995).

SOX9 has been identified as a downstream factor of the WNT pathway in intestinal epithelium, where its expression is restricted to the proliferative lower half of the crypt

(Blache et al., 2004). Furthermore, Blache et al showed that in human colorectal adenocarcinomas SOX9 is strongly expressed in areas that active β-catenin-TCF complexes are found and additionally, that SOX9 expression was undetectable in the intestinal epithelium of TCF4-null mice models.

SOX9 represses Parahox gene caudal type homeobox protein 2 (*CDX2*) and Mucin 2 (*MUC2*). *CDX2* is a tumor suppressor gene (Ee et al., 1995; Mallo et al., 1997) and MUC2 deficiency has been shown to lead to spontaneous intestinal tumors (Velcich et al., 2002). Interestingly, when *CDX2* expression was restored in human colon carcinoma cells, proliferation and soft agar growth of the carcinoma cells was suppressed (Hinoi et al., 2003). Hence, high SOX9 expression in tumors with a constitutive WNT signalling activation could be a contributing factor in cancer progression as well as tumor differentiation levels.

1.3.2 BMP signalling pathway

BMP is part of the TGFβ superfamily of ligands. BMP dimerizes BMP receptor type I and II. This leads mothers against decapentaplegic homologues (SMAD) family of proteins to form trimers that translocate to the nucleus and acts as transcription factors and directly regulates target gene expression. BMP2 and BMP4 are the main BMP receptor ligands in the intestine and are secreted by mesenchymal cells. BMPs promote cell differentiation and counteracts proliferative signals. A balance of proliferation in the base of the crypts and differentiation towards the villi is maintained by regulating BMP signalling. BMP antagonists such as Gremlin 1, Gremlin 2, Chordin-like 1 and Noggin are mainly secreted by myofibroblasts, and smooth muscle cells located underneath the crypt. The higher concentration of these BMP inhibitors at the base of the crypt creates a gradient of increasing BMP from the crypt to the villi. Hence decreasing WNT and increasing BMP signals direct cells to go from and undifferentiated to a differentiated state as they move along the crypt-villus axis.

SMAD4 a human co-SMAD, is commonly mutated in various human cancers. SMAD4 is inactivated in over half of pancreatic duct adenocarcinomas. In colorectal cancer, heterozygous deletion of SMAD4 promoted tumour progression of tumours initiated by inactivation in APC (Zhao et al., 2018).

1.3.3 Notch signalling pathway

Notch signalling is important for maintaining a constant ratio between cell lineages by a mechanism known as lateral inhibition (Sancho et al., 2015). When a cell is activated by Notch signalling, it turns off the production of Notch ligands within the activated cell. Notch ligands are transmembrane proteins and thus direct contact of the membranes between cells are required for Notch signalling. This leads to an ‘on’ or ‘off’ state between neighbouring cells. In the intestinal crypt, Paneth cells express Notch ligands to signal to their CBC neighbours hindering the differentiation of stem cells to the secretory lineage, and by doing so maintains the stem cell population

1.3.4 EGF

EGF as well as TGFα are produced by the Paneth cell as well as the underlying mesenchyme. When EGF signalling is unchecked and overactive, neoplastic growth and cancer formation is more likely. EGF is an important component of the culture medium used to grow intestinal organoids. EGF signal blockade leads LGR5+ stem cells into a quiescent, non-proliferative state and stops intestinal organoid growth (Basak et al., 2017). When EGF signalling is re-established, the stem cells can proliferate as they had maintained their stemness in the absence of EGF signalling.

1.4 Intestinal carcinogenesis

Globally colorectal cancer is the third most common cancer occurring in both sexes combined (Bray et al., 2018). Cancer is not a particular disease but a term that includes various diseases caused by the loss of control over cell proliferation and tumour formation.

Cancer displays certain hallmark characteristics that gives it the growth advantage that marks a well-functioning cancer cell. Sustained proliferative signalling, resisting cell death, activating invasion and metastasis, evading growth suppressors, inducing angiogenesis, deregulating cellular energetics and avoiding immune destruction are some of these hallmarks of cancer (Hanahan & Robert, 2011).

The initiating event in intestinal tumorigenesis is often an activating mutation in the WNT pathway, for example in *APC* or Catenin beta 1. These mutations lead to the stabilization of β-catenin and hence constitutive transcription of WNT pathway target genes by the β-catenin/TCF complex (Bienz & Clevers, 2000). Further mutations such as activation of the Kirsten rat sarcoma viral oncogene (*KRAS*) and inactivation of the tumour suppressor gene *P53*, usually occur in the pathway to cancer formation (Fearon, 1991).

$LGR5^{+}$ stem cells with conditional deletion of *Apc* in mice, results in rapid adenoma formation, whereas TA cells with *Apc* deletion displayed limited expansion and very rarely progressed to adenomas (Barker et al., 2009). Thus, suggesting that the transformation of stem cells, to cancer stem cells by mutations are the origin of tumours.

1.4.1 Intestinal organoids and the tumor organoid model

Intestinal organoid cultures are a useful experimental model. Crypts can be isolated from mouse or human intestine, cultured onto Matrigel, and grown in a medium with a minimum requirement of R-spondin, EGF and Noggin, which simulates conditions of the intestinal stem cell niche (Sato et al., 2009). Isolated intestinal cells undergo anoikis, which is prevented by using Matrigel, which is a matrix rich in laminin and collagen and acts like the basal lamina (Sato & Clevers, 2013).

Crypts are isolated from $Apc^{Min/+}$ tumors and are grown in a medium without R-spondin as $Apc^{Min/+}$ is constitutively WNT active. The R-spondin depletion favours the growth of

tumor organoids and so any remaining healthy crypts are eliminated. These tumor organoids have a spherical organoid structure as the crypt-villus organization is lost. However, epithelial polarity is maintained in the direction towards the lumen. (Langlands et al., 2018).

1.4.2 E-cadherin and its role in cancer

E-cadherin when located in the adherens junctions of cells mediates the adhesion between epithelial cells (Takeichi, 1990). E-cadherin has a cytoplasmic domain that binds to β-catenin or γ-catenin to form complexes with α-catenin. The cadherin/catenin complexes interact with the actin cytoskeleton and is factor in forming tight cell to cell adhesion (Gumbiner & McCrea, 1993).

Epithelium-to-mesenchyme transition (EMT) is one of the initial steps in cancer invasion and metastasis. In this process, epithelial cells acquire characteristics typical of fibroblasts, lose cell polarity, have reduced intercellular adhesion, develop increased motility and increased invasive capacity (Boyer et al., 2000). E-cadherin suppression leads to increased EMT in cancer metastasis (Chen et al., 2017); however, the E-cadherin/catenin complex may also play a role in cancer through its interactions with intracellular signalling pathways involving APC (Rubinfeld et al., 1995). The literature shows that an increased staining of E-cadherin/catenin complex in the cytoplasm is an independent predictor of poor survival in some human cancers (Salon et al., 2005; Wijnhoven et al., 2002). In FAP, there is evidence that expression of E-cadherin and catenins was increased in adenomas with an increase in cytoplasmic localization of E-cadherin and α-catenin (El-Bahrawy et al., 2002).

1.5 Epigenetics

Epigenetics describes heritable phenotypic traits including gene expression, which does not involve mutations in the DNA sequence (Dupont et al., 2009). A variety of factors such as environment, age, disease and lifestyle are capable of influencing epigenetic regulation (Alegría-Torres et al., 2011). Mechanisms that can alter how genes are expressed includes DNA methylation, histone modifications and long non-coding RNAs (lncRNA). DNA methylation occurs when a methyl group is attached to cytosine in the C5 position of CpG dinulceotides. This process silences gene transcription by rendering the DNA inaccessible to the transcription machinery (Jin et al., 2011). Chromatin is formed by the winding of DNA around nucleosomes, where a nucleosome is an octomer containing two of each of the histone proteins H2A, H2B, H3 and H4. These histone proteins have tails on which modifications such as acetyl groups, methyl groups and phosphate groups can be added or removed by histone modifying enzymes (Hyun et al., 2017). Acetylation is carried out by histone acetyl transferases, and acetylation is reversible by histone deacetylases. In a similar manner, histone methytransferases adds methyl groups to the histone tails and is reversed by histone demethylases. Acetylation is usually associated with an open accessible chromatin state. Changes in acetylation and methylation by these enzymes allow for dynamic changes in the activity state of chromatin. Whether the chromatin is in a permissive or repressed state is dependent on the combination of the modification patterns which read as a 'histone code'. This in turn determines whether genes are active or dormant (Jenuwein & Allis, 2001). LncRNAs are

strings of nucleotides that do not code for proteins. They act by interacting with DNA, RNA, proteins and chromatin modifying complexes (Cao, 2014). Thus, the result of epigenetic dysregulation can be the overexpression or suppression of gene transcription, translocations and mutations often associated with cancer (Audia & Campbell, 2016; Baylin & Jones, 2016; Karakaidos et al., 2019). Epigenetic aberrations are potentially alterable and has been identified in all tumour types, leading to a field of research into novel therapies that target restoring the epigenetic landscape in cancer and disease (Greer & Shi, 2012).

1.5.1 LSD1

Lysine specific demethylase 1A (LSD1/KDM1A) is a flavin-dependent oxidase that demethylates mono and di-methyl residues on histone 3 lysine 4 (H3K4) and histone 3 lysine 9 (H3K9). LSD1 consists of a N-terminus SWIRM domain and amine oxidase like domain and a 90-residue insert called the tower domain which divides the amine oxidase like domain into two subdomains (Marabelli et al., 2016). The amine oxidase like-SWIRM subdomain binds to flavine adenine dinucleotide and is specific for protein-protein interactions. The substrate binding subdomain binds to histone 3 as well as various non histone substrates such as protein complexes, transcription factors, receptors and noncoding RNAs (figure 1-3) (Ismail et al., 2018).

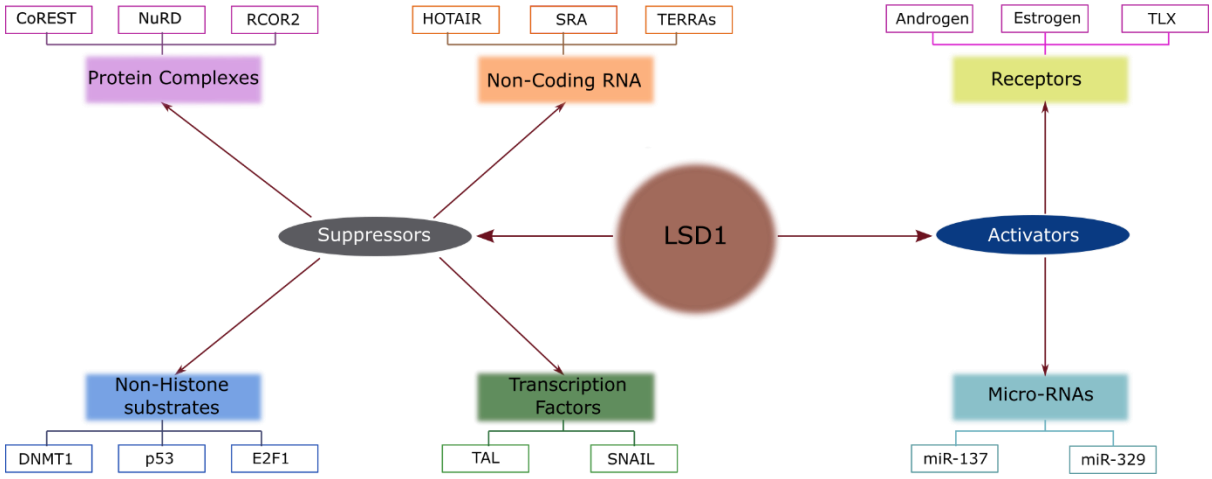

Figure 1-3: Interactions of LSD1 and its functions. Adapted from Ismail et al. Illustrated in Inkscape.

1.5.2 Role of LSD1 in cancer

The overexpression of LSD1 has been seen to promote cancer cell proliferation, migration and invasion of various cancer cells (Cho et al., 2011; Lv et al., 2012). There is increased expression of LSD1 in colon cancer and is significantly associated with higher tumour-node-metastasis (TNM) staging and distant metastasis (Ding et al., 2013). LSD1 is an epigenetic modifier and can interact with various substrates and has diverse functions. Epigenetic dysregulation is emerging as a hallmark of cancer and thus,

epigenetic inhibitors are a therapeutic target of interest. Studies of leukemic and glioblastoma stem cells indicate that LSD1 keeps CSCs in an undifferentiated, therapy resistant state (Karakaidos et al., 2019). LSD1 inhibition has been shown to reduce tumorigenicity in breast, leukemic and glioblastoma CSCs and sensitizes hepatocellular CSCs to treatment (Karakaidos et al., 2019).

In section 1.4.2 we introduced E-cadherin and its role in EMT. LSD1 has a role in this process as well. In colon cancer specimens with a high TNM stage and distant metastasis, a high LSD1 expression has been associated with E-cadherin suppression (Jie et al., 2013). Transcription factors such as Snail family transcriptional repressor 1 (SNAIL) and Snail family transcriptional repressor 2 (SLUG), Zinc finger E-box binding homeobox 1 and 2 and Twist related protein 1 can promote EMT by suppressing the expression of E-cadherin. LSD1 is required in SNAIL/SLUG-mediated transcriptional repression of E-cadherin. In the absence of LSD1, SNAIL and SLUG fail to repress E-cadherin transcription (Ferrari-Amorotti et al., 2013; Lin et al., 2010). The LSD1-CoREST complex interacts with a specific domain of SNAIL/SLUG, which resembles a histone H3 tail like structure and hence acts as a molecular hook that brings the complex to the E-cadherin gene promoter. SNAIL/SLUG binds the E-box elements of the E-cadherin promoter through their zinc-finger motifs. The LSD1-CoREST complex causes demethylation of the H3K4me1/2 at that site causing suppression of E-Cadherin transcription (Baron et al., 2011; Ferrari-Amorotti et al., 2013; Lin et al., 2010).

Another important LSD1 interaction is with the tumor suppressor p53. LSD1 is capable of repressing p53 mediated tumour cell apoptosis. LSD1 demethylates p53 lysine 370, upon which p53 loses the ability to bind to P53 binding protein 1, resulting in the loss of transcriptional activation that supports apoptosis. (Huang et al., 2007).

High LSD1 expression levels have been associated with high expression levels of LGR5 in CRC tissue. Furthermore, it has been shown that in a study of LSD1 inhibition using CBB1003 on CRC tissue resulted in downregulation of LGR5 and the subsequent inactivation of WNT/β-catenin pathway; specifically, β-catenin/TCF signalling. (Hsu et al., 2015). Thus, based on the literature LSD1 likely has a role in increasing WNT activation in CRC.

Recently published data from our research group demonstrate that Inhibition of LSD1 by GSK-LSD1 in *Lgr5*-EGFP derived intestinal organoids led to an expansion in $LGR5^+$ cells, while resulting in a loss of Paneth cells (Zwiggelaar et al., 2020). As we have discussed earlier Paneth cells provide stem cell niche factors such as WNT3a which are necessary for organoid growth and for stemness. Therefore, the successful growth of LSD1 inhibited organoids which are devoid of Paneth cells without external WNT supplementation is unexpected. Zwiggelaar et al further demonstrated that in an intestinal epithelial cell specific LSD1 knock-out mouse model, WNT blockade achieved by using the porcupine inhibitor IWP-2 resulted in sustained growth of KO organoids compared to WT, though growth rate was reduced. Tough these KO organoids appear very similar to fetal derived organoids, there are clear differences. Unlike fetal spheroids, KO organoids required R-spondin 1 for growth. Also, KO organoids form crypts/villus structures whereas both fetal organoids and WNT supplemented organoids form spheroids. This might indicate that the adult KO epithelium has a behaviour midway between that of fetal and adult intestinal epithelial cells (Zwiggelaar et al., 2020)

LSD1 appears to have a role in cytoskeletal organization and in particular is associated with the upregulation of FLNA. Zwiggelaar et al found that genes upregulated in LSD1 KO crypt cells is associated with increased H3K4me1 levels at putative enhancer sites. Parmar et al showed that increased H3K4me1 levels also resulted in functional changes in chromatin accessibility by performing an Assay for Transposase-Accessible Chromatin using sequencing comparing the intestinal crypts of LSD1 WT and KO. Of interest, genes associated with cytoskeletal organization such as *Flna* were affected by this mechanism. Increased protein levels of Filamin A (FLNA) were found in LSD1 KO organoids and organoids that were treated long-term with GSK-LSD1 inhibitor (Naveen Parmar et al., 2021; Zwiggelaar et al., 2020).

2 Objective

LSD1 is an epigenetic modifier and can interact with various substrates and has diverse functions. LSD1 affects ISC biology and WNT signalling pathways. Recently published data from our research group show that LSD1 KO organoids can grow in the absence of WNT signalling (by IWP-2 treatment) despite the loss of Paneth cells. In addition, GSK-LSD1 treated intestinal organoids have a higher number of *Lgr5*-EGFP positive cells indicating that the *Lgr5*+ population is independent of WNT (Zwiggelaar et al., 2020). Furthermore, epigenetic dysregulation is an emerging hallmark of cancer and thus, epigenetic inhibitors are a therapeutic target of interest. We therefore want to investigate the role of LSD1 of WNT driven intestinal tumors by using an organoid tumor model to look at changes in tumor morphology and the expression of cytoskeletal proteins and WNT pathway factors.

3 Methodology

3.1 Mouse models

Apc $^{Min/+}$ mouse strain (stock no: 002020) were obtained from Jackson Laboratories. *Lgr5*-CreERT2 *Apc*$^{f/f}$ *Lsd1*$^{f/f}$ (*Lgr5*-CreERT2 from Jackson, *Apc*$^{f/f}$ also Jackson (stock: **029275)**, *Lsd1*$^{f/f}$ mice a kind gift from Dr. Stuart Orkin. All mice were housed in sterile conditions and maintained by the Comparative Medicine Core facility at NTNU. The Norwegian Food and Safety Authorities (FOTS) evaluated and ethically approved all experiments performed on mice.

Lgr5-CreERT2 Apc$^{f/f}$ (*Apc*KO) and *LSD1*$^{f/f}$ (LSD1 KO) are used in our experiments. To create these strains firstly, a heterozygous mouse with a *Lgr5*$^{EGFP\text{-}IRES\text{-}CreERT2}$ knock-in allele which deletes the *Lgr5* gene function while expressing EGFP and a Cre-ERT2 fusion protein is generated. This line is crossed with a mouse containing a locus of X over P1 (*loxP)*-flanked sequence of interest, in this case either *Apc* or *LSD1*. The Cre-ERT2 fusion protein is a Cre recombinase fused to a mutant estrogen receptor, which binds to tamoxifen. Introduction of tamoxifen allows the Cre-ERT2 enzyme to enter the nucleus and excises the floxed sequences in *Lgr5* expressing cells (Koo & Clevers, 2014).

3.2 Tissue fixation and processing

Fixation is necessary after harvesting living tissue from an organism as it will deteriorate from its original state rapidly. To obtain accurate results on further analysis tissue should be preserved in as close to life-like condition as possible. Tissue is usually preserved through immersion in a fixative solution such as formaldehyde, which behaves as an enzyme blocker. Formaldehyde fixates tissue by forming crosslinks between various biomolecules preserving them spatially. Paraformaldehyde (PFA) which is polymerized formaldehyde is preferred to formaldehyde as it is more reliable and purer (Cook, 2015).

Fixated tissue is embedded in paraffin wax which gives added support to the tissue. Paraffin wax has a melting point of 60°C and is solid at room temperature. Paraffin wax is also immiscible with water. Thus, embedment is a multistep process, which firstly involves the removal of water by dehydration, and secondly clearing, where the dehydrating agent is replaced with a wax miscible reagent. In the final step tissues are impregnated with wax. The paraffin impregnated tissue is then placed in a mould where the wax can solidify (Cook, 2015).

3.2.1 Experimental procedure

The small intestine and colon were harvested from euthanized mice, measured, and divided by visual judgement into duodenum, jejunum, ileum and colon. The swiss roll method was used; sections were cleaned with phosphate-buffered saline (PBS), sliced open longitudinally and rolled onto wooden sticks with the mucosal side facing the outside (Moolenbeek & Ruitenberg, 1981). Tissue samples were fixated in 4% PFA

overnight. Tissue processing was done automatically by a Lecia ASP300S tissue processor, and then embedded in paraffin. Sections were sliced using a microtome into 4μm thick sections and placed on glass slides using flotation. Sections of ileal and jejunal swiss rolls were subsequently stained using hematoxylin and eosin and immunofluorescence staining methods.

3.3 Hematoxylin and eosin staining

One of the primary methods used in histology is that of hematoxylin and eosin (H&E) staining. Hematein the oxidized form of hematoxylin is the active colorant which forms a stain when combined with a metallic salt: a mordant; usually an aluminium salt (Cook, 2015). This forms a basic and positively charged solution which stains acidic and negatively charged structures such as DNA and RNA. This turns the cell nucleus blue or dark-purple. Eosin is used as a counterstain to hematoxylin and is an acidic and negative dye, which will stain basic and positively charged structures, such as the cytoplasm and extracellular matrix a few shades of pink and red (Cook, 2015). It is essential that paraffin wax is removed and the tissue to be stained rehydrated prior to staining as the aqueous staining solutions are immiscible with wax.

3.3.1 Experimental procedure

Paraffin wax was removed, and the tissue rehydrated. Tissue sections were warmed to 60°C for 30 mins in an oven. It was then placed in neo-clear (this is preferred to the more toxic xylene) twice for 5 minutes each. The rehydration process was carried out by transfer through graded percentages of alcohol (100%, 96% and 70%) for approximately 1 minute each before placing in water. Staining of tissue done by placing in hematoxylin for approximately 1 minute and then washing in warm water to remove the excess, followed by placing slides in eosin for 5 minutes and washing in warm water. Tissue sections were dehydrated by placing in increasing gradations of alcohol (80%, 96%, 100%) and finally in neo-clear. Slides were then mounted using aqueous mounting medium and coverslips applied.

3.4 Immunofluorescence

Immunofluorescence (IF) is a technique where an antibody can be labelled with a fluorochrome and hence visualized under a fluorescent microscope. The main principle behind this technique is that antibodies bind specifically to antigens in biological tissue and allow for detection and localization of target proteins. Primary or direct IF uses a single fluorochrome-conjugated primary antibody that directly binds to the epitope of interest. Another technique is secondary or indirect IF which utilizes two antibodies. The first unlabelled antibody binds to the target epitope, and the secondary antibody is tagged with the fluorophore and binds to the primary antibody. By using the indirect method, signal amplification can be achieved. This is advantageous in situations where the target protein is not highly expressed, by through signal amplification can be better detected (Im et al., 2019).

Fixation and processing of the tissues can alter the antigens and so before IF staining can be carried out, the full immunoreactivity of the tissue sections must be restored (Leong & Leong, 2007). A technique called antigen retrieval is used to unmask the antigen and involves the use of either enzyme or heat (Im et al., 2019; Kim et al., 2016). In heat retrieval the sections are placed in a buffer solution and heated in a microwave. Depending on the antigen and the fixation method, the amount of time required and the power at which heating takes place varies (Gu et al., 2016; Im et al., 2019).

Blocking is a necessary step before incubation with primary antibodies. All potential nonspecific bindings sites in tissue needs to be blocked to prevent antibodies from binding to them. An ideal blocking solution would have no specific affinity for the target epitopes. Serum from the source species of the secondary antibody is an important aspect of a blocking solution (Li-Cor, 2017). The natural host serum carries antibodies that bind to reactive sites and prevents nonspecific binding of the secondary antibodies used in the assay. In addition to host serum, blocking solutions usually contain bovine serum albumin (BSA) or non-fat dry milk which also binds to nonspecific sites (Im et al., 2019). Permeabilization is another important step, this allows the intracellular structures to become accessible to the antibodies used. Triton X-100 and NP-40 are classical detergents commonly used, along with Tween20, saponin and digitonin (Cook, 2015). Before primary and secondary antibodies are added to the tissue they are usually diluted in a buffer, containing blocking solution components to improve antibody stability and tissue diffusion (Kim et al., 2016).

3.4.1 Experimental procedure

Tissue sections were deparaffinized by heating in an oven at 60°C for 30 mins in an oven. It is then transferred into neo-clear for 5 minutes twice before rehydration through transferring the sections through a series of gradually decreasing concentrations of ethanol; 100%, 96% and 70% for 3 mins each. It is finally rehydrated fully by placing in water for 3mins. Antigen retrieval is carried out by covering the tissue sections with a pH 6 citrate buffer and then heated in a microwave at 800W until boiling and then at 90W for 15mins. Sections are then cooled in the buffer at room temperature for 20 mins.

Slides were then washed in water for 2 minutes. Tissue sections were suctioned dry carefully and marked with a hydrophobic pen. A blocking buffer consisting of 2% normal goat serum (NGS), 1% BSA, 0.2% Triton X-100 and 0.05% Tween 20 in 1x PBS was added to each tissue section incubated under a lid in a humid chamber for 1 hour at room temperature. The hydrophobic pen kept the buffer solution contained and prevented dehydration. The primary and secondary antibody solutions were diluted in the same blocking buffer solution. The blocking buffer was removed by suctioning after 1 hour and the primary antibody solutions were added; LSD1 (Cell signaling #21845) Rb monoclonal antibody in a 1:200 dilution, β-Catenin (Santa Cruz # 130917) mouse antibody in a 1:100 solution and CD31 (Millipore # MAB1398z) Hamster monoclonal Antibody in 1:200 dilution. Slides were then incubated overnight in a humid chamber at 4°C.

The slides were washed 3 times with agitation with Tris-buffered saline and Tween (TBST) the next day. The following secondary antibodies were used: Goat anti- Rabbit

IgG Alexa Fluor 488 (Invitrogen, #A-11034) in a 1:500 dilution, Goat anti-Mouse IgG Alexa Flour 555 (Invitrogen, #A21422) in a 1:500 dilution, Goat anti-Hamster IgG Alexa Fluor 647 (Invitrogen, #A-21451) in a 1:500 dilution and Hoechst 33342 (ThermoFisher Scientific #62249) in a 1:5000 dilution for 1 hour in room temperature.

After LSD1, Beta Catenin and CD31 IF staining, the tissue slides were imaged (see section 3.7 Microscopy and imaging).

3.5 *Apc*$^{Min/+}$ tumor isolation and culture of intestinal organoids

Intestinal organoid cell culture is a new method of utility in the study of intestinal function and cellular processes. This is a method that allows for greater physiologic modelling of intestinal response to various stimuli when compared to more traditional two-dimensional cell line cultures (Wallach & Bayrer, 2017). As mentioned in section1.4. a combination of growth factors; EGF, noggin, and R-spondin is essential to maintain intestinal stem cells *in-vitro* and hence intestinal organoids. When derived from healthy intestinal epithelium, crypts form organoids which are composed of a central cystic structure surrounded by budding crypt like structures. At the bottom of the crypt-like structures are intestinal stem cells and Paneth cells. The enterocytes that have undergone mitosis migrate towards the center of the cyst and are shed into the lumen (Sato & Clevers, 2013). To selectively enrich for tumor organoid cultures, isolated *Apc*$^{Min/+}$ intestinal tumors are cultured in a medium without R-spondin as these organoids are WNT driven and independent of R-spondin

3.5.1 Experimental Procedure

Apc$^{Min/+}$ tumour isolation and culture.

Small intestine was harvested from an *Apc*$^{Min/+}$ mouse and washed in PBS. The intestine was opened longitudinally and approximately 10 well defined tumors were excised carefully avoiding taking normal tissue. The excised tumors were washed approximately 10 times in PBS. It was then incubated in 2mM EDTA in 40ml PBS at 4°C with agitation. Tumors were cut further into smaller pieces and incubated in 0.5mg/ml collagenase/dispase at 37°C for 20 min with intermittent inversions. A 18G wide bore needle was used to syringe the tumors once or twice to break it up further before mashing in through a 70μm cell strainer. The cells were washed multiple times in PBS by spinning down at 400g for 5 mins at 4°C each time and discarding supernatant. Isolated cells were seeded by resuspending in 40μl of Matrigel (Corning, 734-1101) per well in a 24 well plate. The polymerized domes of Matrigel were bathed in 500μl Basal culture medium (BCM) solution made with Advanced DMEM/F12 (Life Technologies) supplemented with 2mM Glutamax (Life Technologies), 10mM HEPES, 100 U/ml penicillin/ 100mg/ml streptomycin and supplemented with N2 (Thermo Fisher, 17502048), B-27 (Thermo Fisher, 17504044), N-acetyl-L-cysteine (Sigma, A7250), 50ng/ml murine EGF (Thermo Fisher, PMG8041) and 10% Noggin conditioned medium. This supplemented medium is referred to as BCM-EN.

Response of LSD1 WT and KO intestinal organoids to WNT enhanced conditions.

The response of LSD1 wild type (WT) and knock out (KO) organoids to added WNT3a and CHIR-99021 (CHIR) conditions was studied by passaging and seeding both LSD1 WT and KO organoids in control conditions of BCM-ENR, BCM-ENR with 25% WNT3a and BCM-ENR with 3μM CHIR99021. BCM-ENR consists of the above mentioned BCM-EN supplemented with 20% R-spondin conditioned medium. Images were taken using Z-stack at 2x and 4x magnification for analysis of size and morphology over the course of the experiment from day 1 to 4. Whole cell lysates were taken at 24hrs and day 4 for western blots. Experiments were repeated three times in total.

Response of *Apc*$^{Min/+}$ intestinal tumour organoids to LSD1 inhibition.

Apc$^{Min/+}$ and *Apc*KO organoids were seeded in different conditions: BCM-EN, BCM-EN with 5μm GSK-LSD1 inhibitor and BCM-EN with 100nm ORY-1001 LSD1 inhibitor. Images were taken using Z-stack at 2x and 4x magnification for analysis of size and morphology over the course of the experiment from day 1 to 5 for *Apc*$^{Min/+}$ experiments and day 1 to 4 for *Apc*$^{Min/+}$ and *Apc*KO experiments. Whole cell lysate was extracted on day 4 for western blots from *Apc*$^{Min/+}$ and *Apc*KO experiments. *Apc*$^{Min/+}$ experiments were repeated three times in total. Subsequently, *Apc*$^{Min/+}$ and *Apc*KO experiments were repeated twice.

3.6 Staining of organoids

An important step is permeabilization and blocking. The permeability and blocking buffer of PBS-TX100 0.2%, glycine 100mM, BSA 1% and NGS 2% is used. Glycine is an amino acid with negative charge that binds unbound aldehydes to reduce background fluorescence. Normal goat serum and Bovine serum albumin block unspecific binding sites.

3.6.1 Experimental Procedure

Apc$^{Min/+}$ and *Apc*KO organoids were passaged and seeded in Matrigel onto an eight well μ-slide (ibidi, #80826) in three different conditions: 2 wells as controls with BCM-EN medium, 3 wells with BCM-EN + 5μm GSK LSD1 inhibitor and 3 wells with BCM-EN + 100nm ORY-1001 LSD1 inhibitor.

After completion of 5 days with treatment each well of the ibidi plates were fixed for 45mins in a 4% PFA, 2% sucrose solution and washed in PBS thrice for 5mins and stored in PBS at 4°C. Permeabilization and blocking done using PBS-TX100 0.2% + Glycine 100mM + BSA 1% + NGS 2% for 2 hrs at room temperature. Primary antibodies were added to PBS-TX100 0.2%, BSA 0.5% and NGS 1% solutions. The wells were washed twice in PBS for 5 mins before incubating with the primary antibody solutions: β-catenin (BS Biosciences #610154) mouse monoclonal antibody in a 1:200 dilution, E-cadherin (Cell signaling #3195) rabbit monoclonal antibody in 1:200 dilution, Sox 9 (Merck

AB5535) rabbit polyclonal antibody in 1:200 dilution and Filamin A (Invitrogen PA582043) rabbit polyclonal antibody in 1:200 dilution at 4°C overnight in agitation.

Wells were washed 3 times for 10 mins each using PBS-Tween 0.1% at room temperature in agitation. It was then incubated in a PBS-Tx100 0.2%, BSA 0.5% and NGS 1% solution with secondary antibodies: Goat anti- Rabbit IgG Alexa Fluor 488 (Invitrogen, #A-11034) in a 1:500 dilution, Goat anti-Mouse IgG Alexa Flour 647 (Invitrogen #A-21236) in a 1:500 dilution, Phalloidin-Rhodamine conjugate (Invitrogen #R415) in a 1:100 dilution, Hoechst (ThermoFisher Scientific #62249) in a 1:1000 dilution and Ulex europaeus agglutinin-1 (UEA1 Vector Laboratories RL-1062) in a 1:1000 dilution overnight in agitation at 4°C. Wells were then washed three times for 10mins each using PBS-Tween 0.1% at room temperature in agitation. Distilled water was added to wells for 5 mins at room temperature. Specimens were then mounted in 150μl of Fluoromount G (Thermo Fisher Scientific). Images were acquired using LSM880 Airyscan confocal microscope (Zeiss) at 20x magnification.

3.7 Microscopy and Image Analysis

In light microscopy, a system of lenses in combination with visible light is used to create a magnified image of a small object. Light is focused onto a specimen using a lighting system and a condenser lens. The light is picked up by the objective lens above and focused onto the focal plane. In combination with the ocular lens which is the eyepiece a magnified image of the specimen is created (Cook, 2015).

Fluorescence microscopy is frequently used in histology to study various elements tagged with fluorescent probes. Fluorescence occurs when the light absorbed by a fluorophore loses energy and the emitted light has a longer wavelength as a result. This difference is known as the Stokes shift (Cook, 2015). A fluorescent microscope has two filters, one positioned above the specimen and the other below. The filter below the specimen absorbs the long wavelengths. allowing only short wavelengths to pass through and illuminate the specimen. The second filter behaves as a barrier that absorbs all the short wavelength light allowing only the longer wavelengths to pass through, hence transmitting the emitted fluorescence. In addition, it is possible to illuminate the specimen from above using a dichroic mirror and the objective used as a condenser in what is known as epifluorescence. This has advantages over transmission fluorescence such as better resolution and reduced fading of the specimen as only a small area is illuminated when viewed (Cook, 2015; Thorn, 2016).

Confocal microscopy utilizes a very small aperture (a pinhole) which restricts out-of-focus light to produce an image with very high signal to noise ratio. However, since only a very small area is examined at a time, the specimen must be scanned by use of a laser beam and the full image is reconstructed. An added benefit to confocal microscopy is the ability to image a thin plane of the specimen. By imaging several optical sections in a stepwise manner to form a Z stack, three dimensional microscopy is possible (Cook, 2015).

3.7.1 Experimental procedure

H&E stained *Apc*$^{Min/+}$ specimens were imaged using EVOS FL Auto 2 Cell Imaging System (Thermo Fisher) with an EVOS™ Achromat 10x objective and an Olympus 20x Super-Apochromat objective. Overall morphology and characteristics of the tumours formed in the *Apc*$^{Min/+}$ mouse model were thus identified.

Live organoids under the varying treatment conditions as described in above experiments were imaged at regular intervals with 2x objective (EVOS™ LPlan 2x/0.06) and 4x objectives (EVOS™ Plan Fluo 4x/0.13) with Z-stacks to study size, morphology and counts using a standardized script for quantification as described in Lindholm et al (2020). Every image was viewed to ensure that classification and segmentation of the organoids were adequate. Manual adjustments of counts were made for assessment of budding in *LSD1* WT and *LSD1* KO organoids as there was wrongful classifications from the standardized script (Lindholm et al., 2020). To assess ellipticity, for each organoid the major axis length (A) and the minor axis length (B) was measured using ImageJ, and the ratio (A/B) was calculated. The mean value of A/B per well was then used as a measure of the ellipticity seen in each well. When A/B = 1 an organoid was considered circular. An organoid was more elliptical the greater than 1 the ratio of A/B was.

Images of *Apc*$^{Min/+}$ tissue sections with immunofluorescent stains for LSD1 labelled with Alexa Fluor 488 (green), β-catenin labelled with Alexa Fluor 555 (magenta), CD31 labelled with Alexa Fluor 647 (red) and Hoechst 33342 (blue) were obtained using LSM880 Airyscan confocal microscope (Zeiss) with a Zeiss 10x objective (Plan-Apochromat 10x/0.40) a Zeiss 20x objective (Plan-Apochromat 20x/0.8).

Images of *Apc*$^{Min/+}$ and *Apc*KO organoids with LSD1 innhibitors with IF stain for β-catenin labelled with Alexa Fluor 647 (magenta), E-cadherin labelled with Alexa Fluor 488 (green), SOX9 labelled with Alexa Fluor 488 (green), Filamin A labelled with Alexa Fluor 488 (green), Phalloidin-Rhodamine conjugate for F-actin (red), UEA1 (red) and Hoechst 33342 (blue) were obtained using LSM880 Airyscan confocal microscope (Zeiss) and a Zeiss 20x objective (Plan-Apochromat 20x/0.8) in Z-stack.

Fluorescence intensities of proteins of interest was measured by generating sum slices of a z stack of images for each organoid. Thresholds were applied to the images and intensities were measured for the protein of interest, then normalized against the intensities measured for Hoechst 33342. ImageJ version 1.53K was used for processing the images and measuring intensities (Schneider et al., 2012).

3.8 Western blot and protein quantification

Protein quantification

Protein quantification is done using the Pierce ™ bicinchoninic acid (BCA) Protein Assay kit (Thermo Fisher), which is a colorimetric assay with a linear working range for BSA of 20 to 2000 μg/mL. Protein in an alkaline medium reduces the cation Cu2+ to Cu1+, the BCA Protein Assay utilizes this principle along with the selective colorimetric detection of Cu1+ by BCA (Smith et al., 1985; Thermo-Fisher, 2017). In the first step, copper is

chelated with protein in an alkaline environment resulting in a light blue complex, which is known as the biuret reaction. The second step in the reaction two molecules of BCA with one cuprous (Cu1+) ion forming an intense, purple-coloured reaction product which is water soluble and exhibits a strong linear absorbance at 562 nm with increasing protein concentrations. This purple complex is about 100 times more sensitive than the pale blue of the first reaction (Thermo-Fisher, 2017).

The presence of cysteine, cystine, tyrosine and tryptophan in the protein´s amino acid sequence has a greater influence on the reaction. However, the universal peptide backbone also has an impact on colour formation which reduces the variability that can result from compositional differences in proteins.

Western Blot

Western blot is a method of separating proteins by gel electrophoresis. The method used is a sodium dodecyl sulphate polyacrylamide gel electrophoresis (SDS-PAGE) system that separates proteins by molecular mass (Hnasko & Hnasko, 2015). Proteins are denatured and secondary and tertiary structures are removed by treatment with reducing agents. The negatively charged SDS coats the protein which results in the protein being anionic. The negatively charged protein migrates towards the positively charged anode within the acrylamide mesh of the gel. Smaller proteins move faster through the gel and hence the proteins are separated by size, which is usually measured in kilodaltons, kDa. The acrylamide concentration impacts the resolution of the gel. To resolve lower molecular weight proteins a higher acrylamide concentration is recommended and to resolve higher molecular weight proteins a lower acrylamide concentration is recommended (Mahmood & Yang, 2012). Samples are loaded into the wells, while reserving one lane for a marker or ladder. These are commercially available mixtures such as Magic Mark and See-Blue that are composed of proteins of known molecular weights that are stained to appear as coloured bands. Because samples have different molecular weights they travel at different rates through the gel and separate into bands when a voltage is applied. These bands can be compared to the bands of the ladder to estimate the protein´s molecular weight.

For the proteins in the gel to be accessed by antibodies the protein bands are transferred to a nitrocellulose (NC) or polyvinylidene difluoride (PVDF). The transfer of proteins can be achieved using a current to pull the negatively charged proteins towards a positively charged anode and onto the NC or PVDF membrane. This transfer maintains the positions of the protein bands from the gel to the membrane. Another method of transfer utilizes capillary action by placing the gel, membrane, and a stack of filter papers in a buffer solution. At this point it is possible to do total staining of the proteins so that they can be visualized (Mahmood & Yang, 2012).

The membrane is selected for its ability to bind protein well and as antibodies are proteins as well as the target, the membrane must be blocked to prevent non-specific binding. This is achieved by soaking the membrane in a dilute solution of protein such as 3-5% bovine serum albumin (BSA) or non-fat dry milk in tris-buffered saline (TBS) and 0.1% of a detergent such as Tween 20 or Triton X-100. The proteins in the blocking solution bind to areas of the membrane where target proteins have not already attached,

allowing the antibodies to bind to the target proteins and not the membrane. Clearer results are achieved by reducing the background signal in this way.

To detect the protein of interest, the western blot is incubated with a primary antibody under agitation for an hour at room temperature or overnight at 4°C. The membrane is then washed in wash buffer to remove unbound primary antibodies. Following this, the membrane is incubated with the secondary antibody, which detects and binds to the species-specific component of the primary antibody. The secondary antibody is linked to horseradish peroxidase (HRP) which utilizes chemiluminescence to detect the target protein. HRP- tagged antibodies will cleave a chemiluminescent substrate when the membrane is incubated with it producing luminescence (Mahmood & Yang, 2012). Chemiluminescence can then be detected using cameras and image analysis software such as used in the LI-COR imaging system. Another method of note involves a near-infrared (NIR) fluorophore-linked antibody. NIR fluorescence detection is a more accurate measure of the signals produced as the light produced is static compared to the more dynamic state of chemiluminescence (Schutz Geschwender, 2012).

3.8.1 Experimental procedure

Apc$^{Min/+}$ and *Apc*KO organoids were passaged and seeded onto a 24 well plate in three different conditions: 2 wells as controls with BCM-EN medium, 2 wells with BCM-EN + 5μm GSK LSD1 inhibitor and 2 wells with BCM-EN + 100nm ORY-1001 LSD1 inhibitor. At the end of the experiment (4 days) whole cell lysate was extracted from both wells of each condition. The whole cell lysates were extracted and stored at -80°C.

10 ml (1% NP-40, 0.02% SDS in 1x TBS) Whole Cell Extract Lysis buffer is prepared with 1 tab of cOmplete™, mini protease inhibitor (Roche) and 1-tab phosSTOP ™ phosphatase inhibitor (Sigmaa Aldrich) and stored on ice at 4°C. Whole cell lysate was prepared by blasting the domes of Matrigel as if to passage. The disrupted domes of Matrigel mixed with medium were collected from wells and transferred to Eppendorf tubes and centrifuged at 4°C, 300g for 5 minutes. Working on ice, the supernatant was discarded from the Eppendorfs and 100μl of the prepared WCE lysis buffer was added and the pellet was resuspended. Samples were allowed to lyse on ice for 10 minutes. Eppendorf tubes were then centrifuged on maximum speed at 4°C for 10 minutes. 75μl of the supernatant (which contains the extracted proteins) was taken off and added to a new Eppendorf tube.

Protein quantification was done using Pierce ™ BCA Protein Assay kit (Thermo Fisher). Protein concentrations in samples and required amount of 4x NuPAGE® LDS sample buffer were calculated and prepared accordingly and heated for 10min at 85°C. NuPage ® 4-12% Bis-Tris Gel was washed twice with distilled water and assembled in tank with 1x MOPS buffer. Protein ladder (4μl See-Blue and 2μl Magic Mark) and samples were loaded into gel wells. Gel was run at 100V, for 15 min and 190V for 60 mins. Using the iBlot2 system the proteins were transferred from the gel to a blotting membrane.

The blotting membrane were then incubated overnight with the primary antibodies in a blocking solution of 5% BSA. Gels were run, blots obtained and incubated with the primary antibodies overnight with agitation at 4°C as such: β-catenin (94kDa) (BS Biosciences #610154) mouse monoclonal antibody in a 1:1000 dilution and GAPDH (37

kDa) mouse monoclonal antibody in 1:5000 dilution. The membranes were washed 5 times for 5min each with agitation with tris-buffered saline with 0.1% Tween 20 (TBST). The secondary antibodies of HRP goat anti-mouse IgG in 1:5000 dilution in TBST or HRP goat anti-rabbit IgG in 1:4000 dilution in TBST was applied to the membranes treated with the corresponding primary antibody and incubated overnight with agitation at 4°C. The membranes were washed 5 times for 5 mins with TBST to remove any unbound antibodies. Imaging was carried out using SuperSignal West Femto (Thermo Fisher Scientific) on a LI-COR Odyssey® Fc imaging system. Signal intensities were measured using the LI-COR software and normalized for comparison.

3.9 Statistical Analysis

To check for significance a one-way ANOVA or two-way ANOVA, with Tukey's post hoc test was performed. All statistical analyses were performed using GraphPad Prism 9.2.0 (GraphPad Software, La Jolla California, USA). Statistical significance at $p < 0.05$; is presented as *p-value < 0.05, ** p-value < 0.01 and *** p-value < 0.00.

4 Results

4.1 LSD1 expression is increased in *Apc*$^{Min/+}$ tumours.

It has been noted in colon cancer that there is increased expression of LSD1, and this is significantly associated with a higher TNM staging and distant metastasis (Ding et al., 2013). As we would like to study the role of LSD1 in WNT driven tumors, we first characterise the phenotype displayed in *Apc*$^{Min/+}$ tumors by examining H&E stained transverse sections of ileal and jejunal swiss rolls harvested from *Apc*$^{Min/+}$ mice under bright light.

Apc$^{Min/+}$ tumours can be identified by its histological characteristics. The normal intestinal architecture of crypt villus units is disrupted by a trapezoid shaped area of densely stained dysplastic epithelium. The cells within the adenoma are enlarged and crowded with large pleomorphic nuclei and increased nuclear to cytoplasmic ratio. Most of the adenomas appear broad based, with some appearing pedunculated (Figure 4-1).

To visualise LSD1 protein levels in tumor tissue compared to normal tissue in *Apc*$^{Min/+}$ transverse tissue sections of swiss rolls were stained for LSD1 (green), β-catenin (magenta), CD31 (red) and the nuclei stained blue. Total LSD1 staining was seen to be increased in the tumours, and the β-catenin distribution was more cytoplasmic/nuclear compared to normal tissue where it was located at the membrane (Figure 4-2).

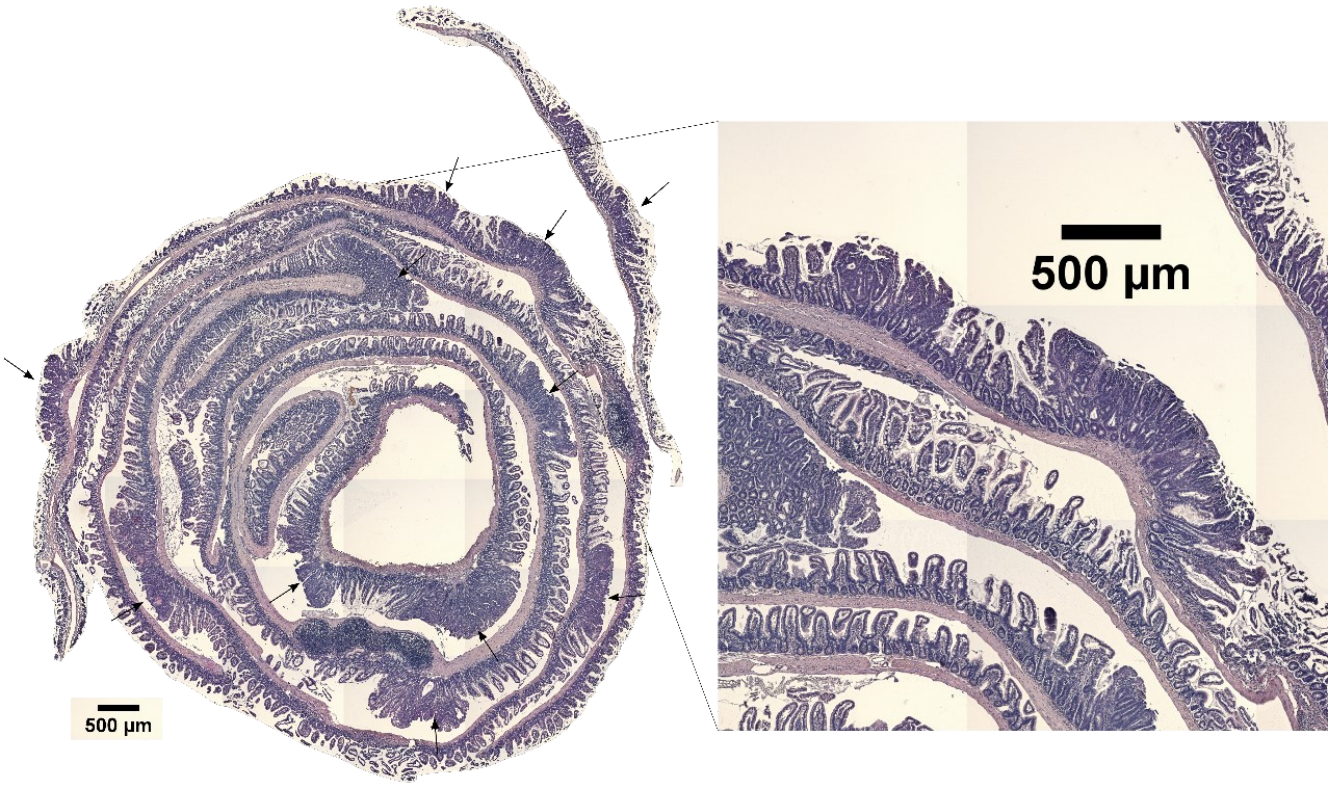

Figure 4-1: *Apc*$^{Min/+}$ mice develop epithelial tumors visible on H&E staining. Representative image of a transversal cut of an ileal swiss roll. Arrows point to tumors, better shown in inset to the right. Images are representative of at least n = 7.

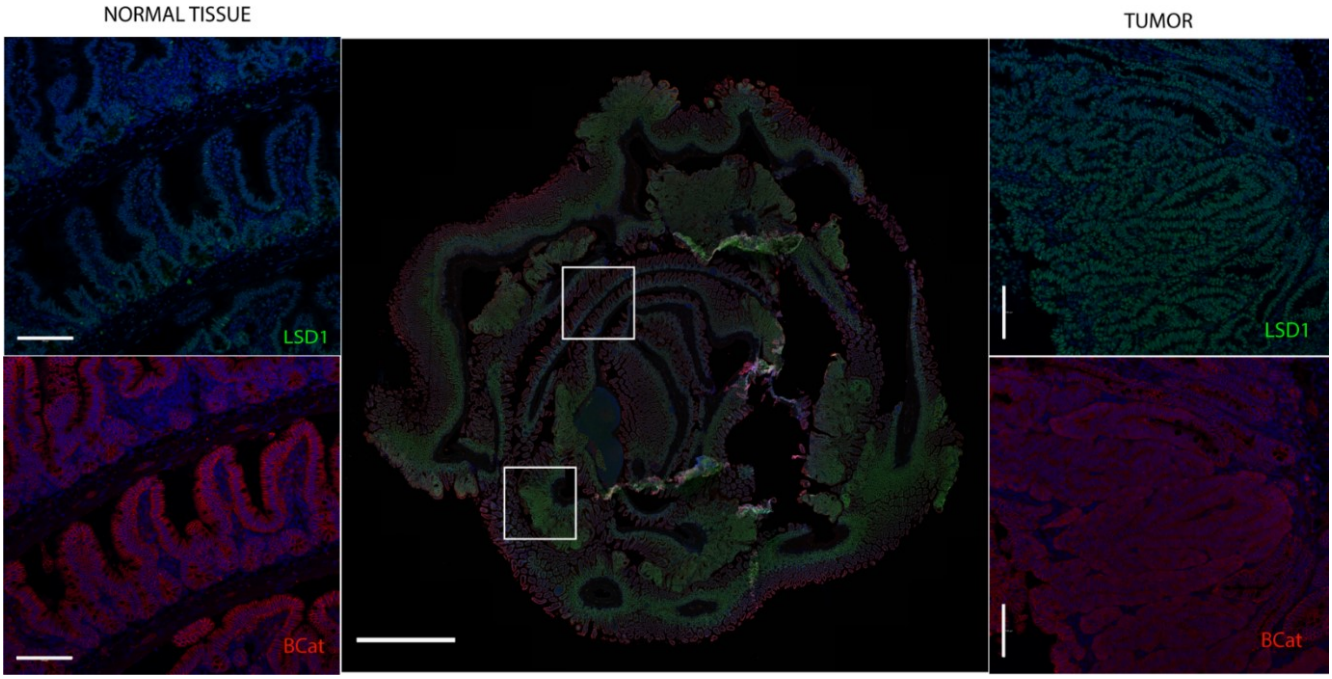

Figure 4-2: LSD1 expression is increased in the tumor tissue of *Apc$^{Min/+}$* mice.
Representative confocal microscopy images of maximum intensity projections of a transversal section of an *Apc$^{Min/+}$* ileal swiss roll immunofluorescent stained for LSD1 (green) and β- catenin (magenta). Blue for Hoechst-stained nuclei and red for CD31. Images are representative of at least n=3. Top square displaying normal tissue better shown in the left insets Bottom square displaying tumor tissue better shown in the right insets. Expression of LSD1 and β-catenin is increased in the tumour tissue compared to the normal tissue. Scale bar represents 2mm for central image and 100µm for insets. Figure mounted courtesy of Mara Martin Alonso.

4.2 LSD1 KO organoids retain a budding phenotype despite WNT enhanced conditions.

It has been discussed earlier in section 1.5.1 that LSD1 inhibited organoids can grow successfully without external WNT supplementation despite displaying a loss of Paneth cells (Durand et al., 2012; Farin et al., 2012; Sato, Stange, et al., 2011; Sato, van Es, et al., 2011). Further strengthening the position that LSD1 inhibited or knockout phenotypes are independent of WNT, WNT blockade by IWP-2 of LSD1 KO organoids still resulted in successful growth (Zwiggelaar et al., 2020). Zwiggelaar et al, also noted that the LSD1 KO phenotype displayed similarities to fetal organoids, however unlike them LSD1 KO organoids formed crypts instead of spheroids.

To study the role of LSD1 in WNT signalling in non tumor organoids, we investigated whether there were any morphological changes between LSD1 KO organoids and LSD1 WT organoids grown in control ENR medium as well as in ENR with added 25% WNT3a and ENR with 3µM CHIR99021. CHIR99021 is a GSK-3 inhibitor and WNT signalling pathway activator (Polychronopoulos et al., 2004; Sato et al., 2004). By comparing

LSD1 WT organoids with LSD1 KO organoids in WNT enhanced conditions, we are trying to identify the impact of LSD1 on WNT signalling.

Figure 4-3 shows that on visual inspection LSD1 KO organoids appear to have more budding and a smaller proportion of spheroidal organoids when exposed to WNT enhanced conditions when compared to WT organoids. LSD1 KO organoids exposed to WNT (WNT3a and CHIR 3µm) were smaller compared to their LSD1 WT counterparts in the same WNT exposed conditions. Furthermore, LSD1 KO organoids formed several large, longer armed crypts than WT (Figure 4-4).

To analyse circularity and mean area, the script described in Lindholm et al was used (Lindholm et al., 2020). Percentage of budding seen in each well of organoids was manually checked and as many budded organoids were mischaracterised as spheroids, manual counts were done to correct for this. Mean area data was used as calculated by the above-mentioned script. Comparing LSD1 WT with LSD1 KO in ENR conditions showed that both groups have a similar percentage of budding organoids. However, in WNT3a 25% and CHIR 3µm treated groups a reduction in percentage of budding was seen in the LSD1 WT genotype compared to the LSD1 KO. It is anticipated that LSD1 WT organoids will become more spherical when exposed to WNT, and the results are congruent with this expectation. In figure 4-5B we see that LSD1 KO organoids have a smaller mean area compared to LSD1 WT on exposure to WNT. WNT exposure usually results in enlarged spheroids in LSD1 WT organoids, and results seen here agree with this. To conclude, WNT exposure results in enlarged spheroids in the LSD1 WT genotype, while LSD1 KO remain similar in size in WNT exposed and untreated conditions and retain a budding morphology on WNT exposure.

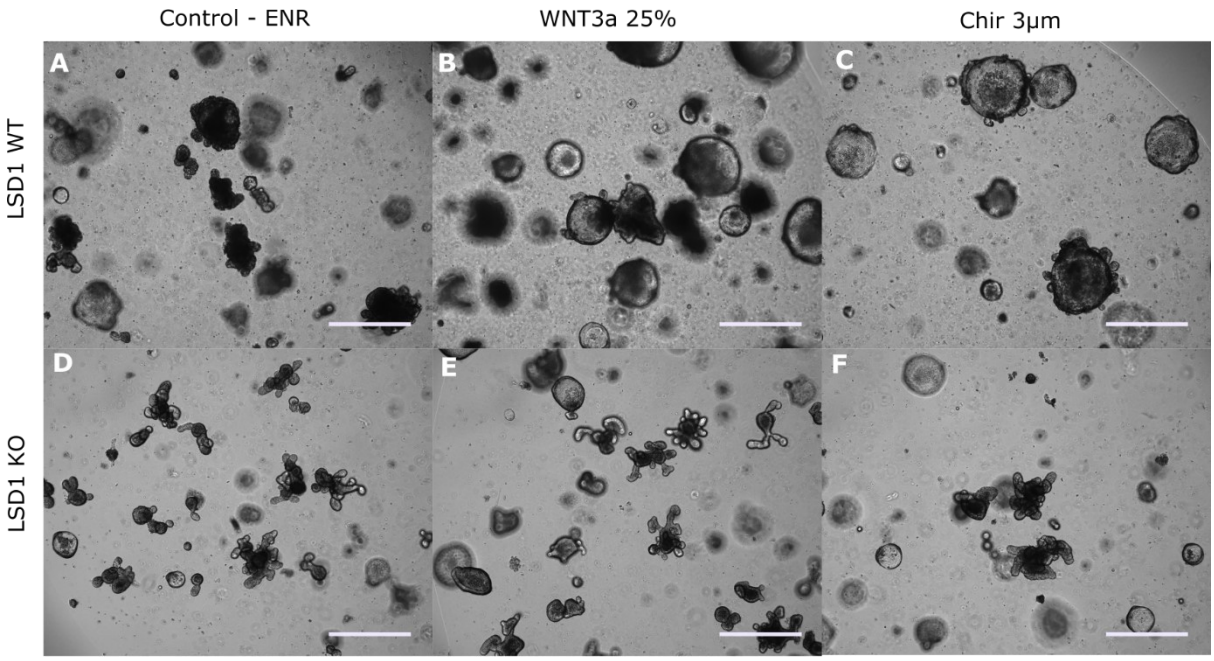

Figure 4-3: LSD1 KO retains a budded morphology despite WNT enhanced conditions. (A-F) Images representative of n = 6 per genotype per condition of LSD1 WT and LSD1 KO organoids on day 4 under treatment conditions. Bright field images. Scale bar represents 625µm.

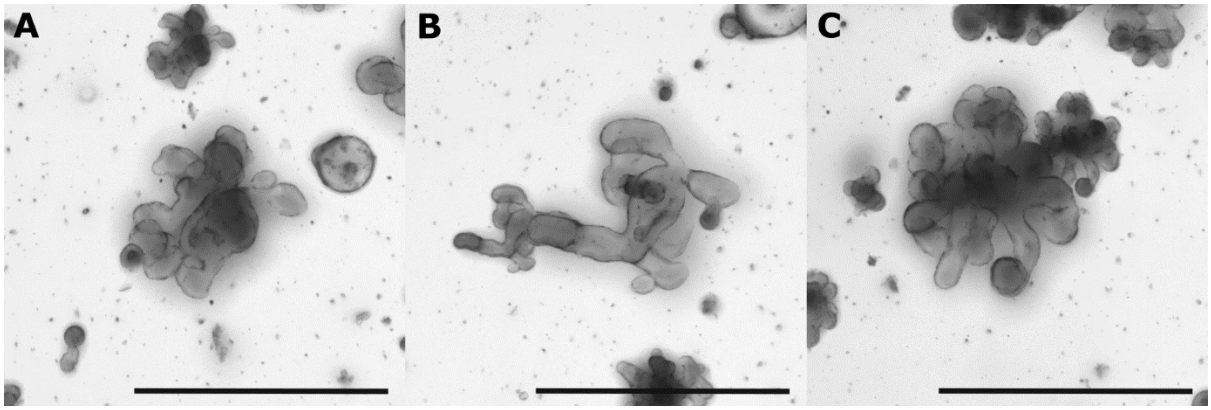

Figure 4-4: LSD1 KO organoids form long crypts under WNT enhanced conditions. (A-C) Magnified images of representative LSD1 KO organoids. A corresponds to ENR, B to Wnt3a 25% and C to CHIR99021 3µm conditions. LSD1 KO organoids retain a budded morphology with multiple long arms of crypts even under exposure to WNT3a and CHIR99021. Bright field images. Scale bar represents 200µm.

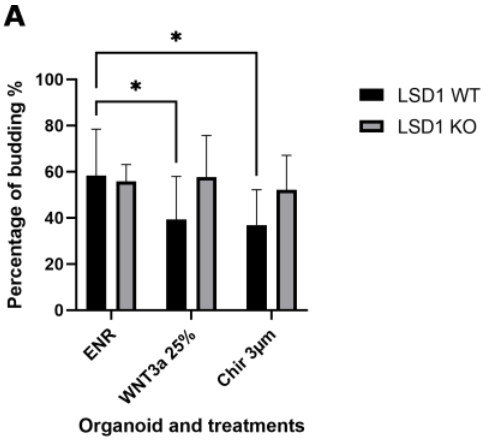

Interaction: F (2, 48) = 2.190 P=0.1230
Treatment: F (2, 48) = 2.797 P=0.0709
LSD1: F (1, 48) = 5.470 P=0.0236*

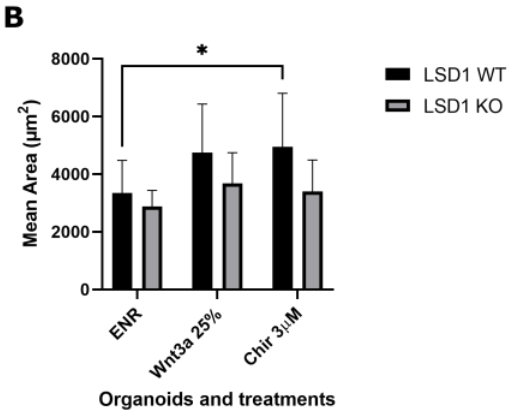

Interaction: F (2, 48) = 0.7786 P=0.4648
Treatment: F (2, 48) = 4.133 P=0.0221*
LSD1: F (1, 48) = 8.431 P=0.0056**

Figure 4-5: LSD1 WT and LSD1 KO in ENR conditions have similar percentages of budding seen. In WNT3a 25% treated and CHIR treated groups a reduction in percentage of budding organoids is seen between LSD1 WT and KO organoids. (A) Graph representing percentage of budding seen in LSD1 WT and KO organoids under ENR, ENR + WNT3a 25% or ENR + CHIR 3µm conditions. *n* = 9 for each condition, per genotype. Numerical data are means ± SD. A similar percentage of budding is seen in ENR treated LSD1 WT and KO organoids. On treatment with WNT3a 25% and CHIR 3µm enhanced ENR, a reduction in percentage of budding is seen in the LSD1 WT organoids compared to the LSD1 KO organoids. (B) Graph representing mean area of LSD1 WT and KO organoids under ENR, ENR + WNT3a 25% or ENR + CHIR 3µm conditions. *n* = 9 for each condition, per genotype. Numerical data are means ± SD. LSD1 KO organoids treated with WNT3a 25% and CHIR 3µm enhanced ENR were smaller than LSD1 WT organoids in the same conditions. (A and B) Percentage of budded organoids and mean area of organoids were calculated per well. Two-way ANOVA with Tukey's post hoc test was performed to determine significance. * P⩽ 0.05, ** P < 0.01, *** P ⩽ 0.001.

4.3 LSD1 inhibition of *Apc*$^{Min/+}$ and *Apc*KO results in morphological changes.

LSD1 is an epigenetic modifier and can interact with various substrates and has diverse functions. Epigenetic dysregulation is emerging as a hallmark of cancer and thus, epigenetic inhibitors are a therapeutic target of interest. Studies of leukemic and glioblastoma stem cells indicate that LSD1 keeps CSCs in an undifferentiated, therapy resistant state. LSD1 inhibition has been shown to reduce tumorigenicity in breast, leukemic and glioblastoma CSCs and sensitizes hepatocellular CSCs to treatment (Karakaidos et al., 2019).

Thus, studying the impact of LSD1 inhibition on a tumor model is of interest. This was achieved by growing *Apc*$^{Min/+}$ organoids in various conditions: BCM-EN, BCM-EN with 5μm GSK-LSD1 inhibitor and BCM-EN with 100nm ORY-1001 LSD1 inhibitor for 4 days. BCM-EN was selected as tumor organoids do not require WNT signalling to grow and so the WNT agonist R-spondin is not necessary in the base medium. Further experiments were carried out using *Apc*$^{Min/+}$ and *Apc*KO grown in BCM-EN, BCM-EN with 5μm GSK-LSD1 inhibitor and BCM-EN with 100nm ORY-1001 LSD1 inhibitor for 4 days to compare difference between those genotypes under LSD1 inhibition.

In figure 4-6 bright field images show that organoids grown in LSD1 inhibiting conditions undergo morphological changes compared to the control group. The LSD1 inhibited organoids developed an ellipsoid (potato-like) shape with dimpling seen along the edges while the control group remained spheroid. These morphological findings were confirmed in *Apc*KO organoids as well as seen in figure 4-7.

The script described earlier in section 4.2 was used to calculate the mean circularity and mean area of the organoids in each well. A trend towards reduction in size on LSD1 inhibition was noted in particular with GSK-LSD1 treated organoids. Mean area of *Apc*$^{Min/+}$ organoids were significantly reduced on LSD1 inhibition compared to control as seen in figure 4-8A. Analysis of mean area measurements of *Apc*$^{Min/+}$ and *Apc*KO organoids however, showed no significant differences between the treatment groups. *Apc*KO organoids were smaller than *Apc*$^{Min/+}$ organoids (figure 4-8B). A different morphology seen as an ellipsoid shaped organoid in LSD1 inhibited organoids is not reflected in the analysis of mean circularity (figure 4-9). As the morphological changes are subtle and the script used has been designed to compare spheroids with budding organoids, it is not surprising that little differences in mean circularity were noted between the organoids and treatment groups using this script.

To better represent the morphology seen in organoids a measure of ellipticity was carried out; the major axis length (A) and the minor axis length (B) was measured using ImageJ, and the ratio (A/B) was calculated for each organoid. The mean value of A/B per well was than used as a measure of the ellipticity seen in each well. When A/B = 1 an organoid was considered circular. The greater than 1 the ratio of A/B, the more elliptical the organoid. Figure 4-10 shows that the LSD1 inhibited *Apc*$^{Min/+}$ organoids are significantly more elliptical than those grown in control conditions of EN.

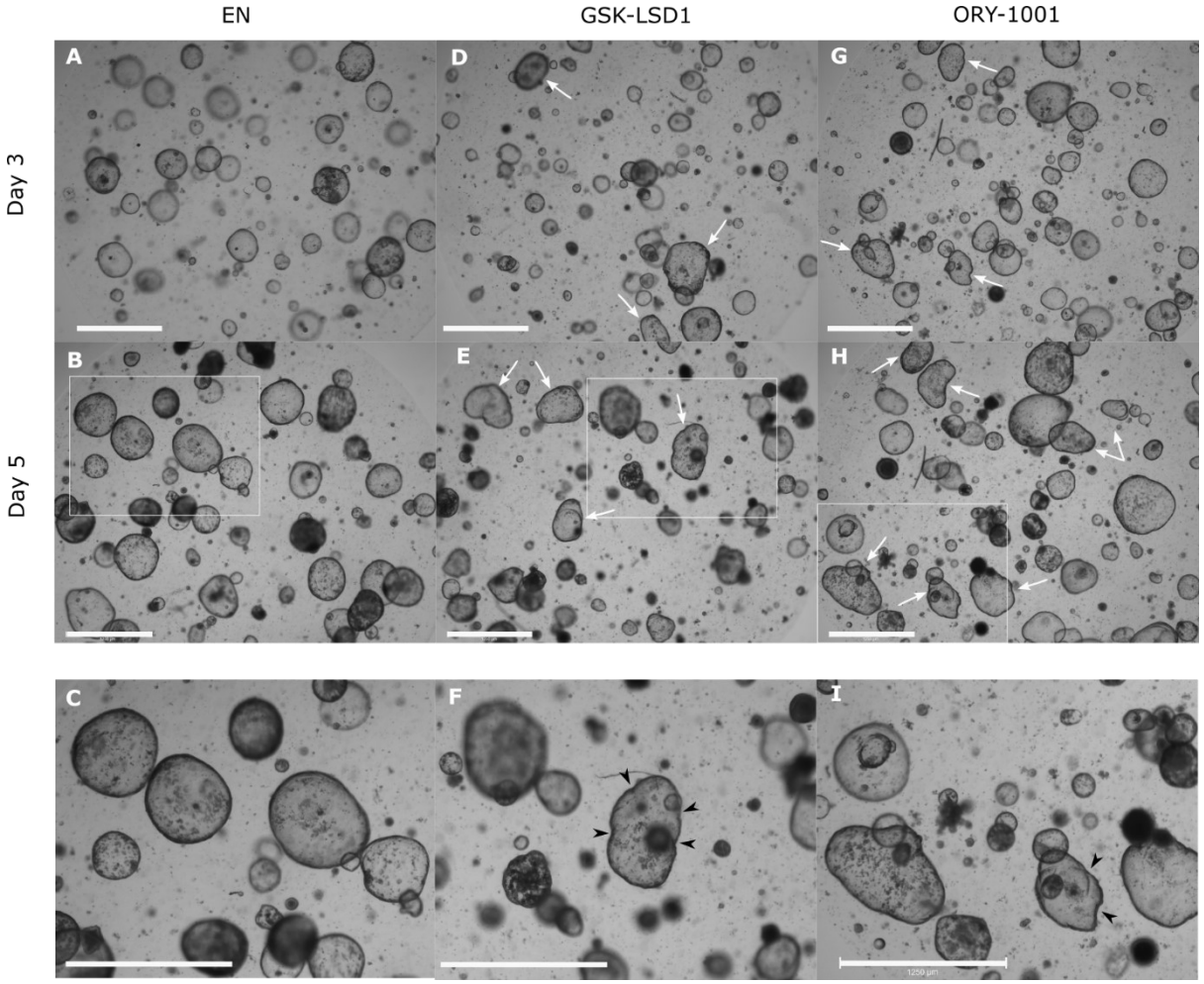

Figure 4-6: *Apc*$^{Min/+}$ under LSD1 inhibition undergo morphological changes and have a more ellipsoid appearance with dimpled edges. Images are representative of at least n = 3 for each condition, with three experimental repeats. Arrows point to organoids with morphological changes. Scale bar represents 1250µm. (A,B) Apc$^{Min/+}$organoids grown in EN (control) are spherical. (C) Enlarged section of the inset in (B) showing organoids maintain a spherical structure at day 5 in EN medium. (D,E) *Apc*$^{Min/+}$organoids grown in medium with GSK-LSD1 undergo morphological changes. Organoids have an ellipsoid (potato-like) shape with dimpled edges. (F) Enlarged section of the inset in (E) with arrowheads showing dimpling at the edges. (G,H) *Apc*$^{Min/+}$ organoids grown in medium with ORY-1001 display morphological changes compared to control organoids as well. Potato-like shapes with dimpled edges seen. (I) Enlarged section of inset in (H) with arrowheads showing dimpling along the edges of an organoid.

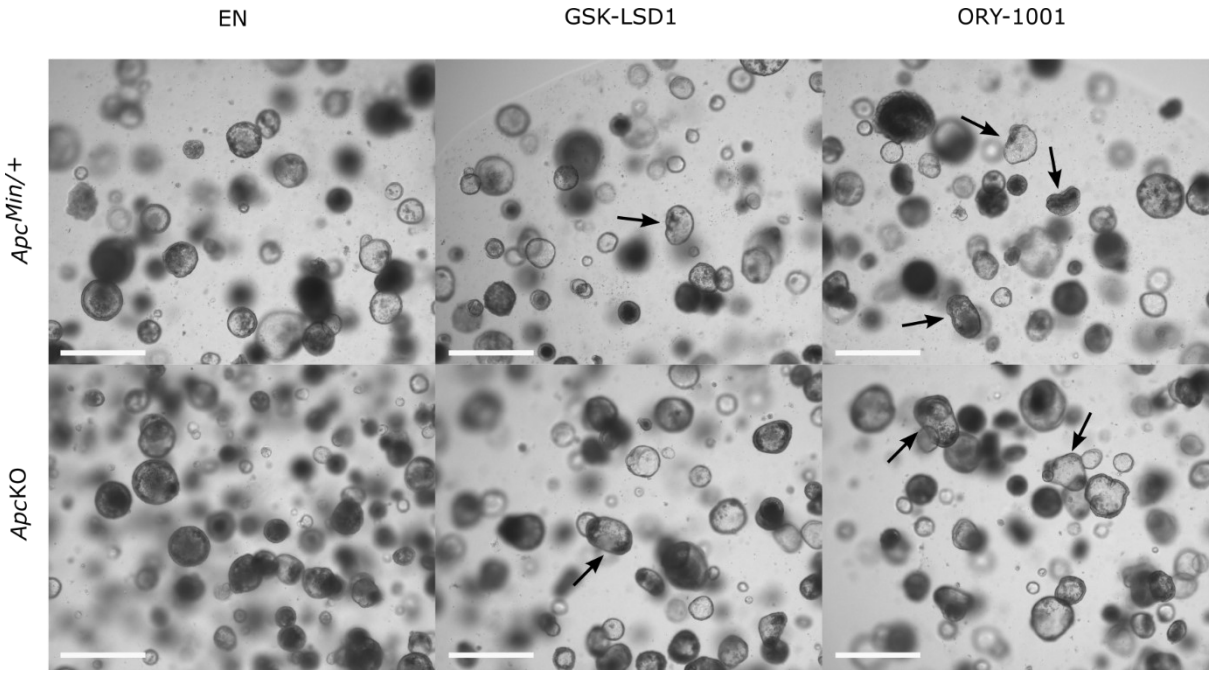

Figure 4-7: *A*pcKO organoids result in similarly potato shaped and dimpled organoids as *Apc*$^{Min/+}$ organoid when grown in LSD1 inhibiting conditions. Image of organoids on day 4 after exposure to EN, EN + GSK-LSD1 and EN + ORY-1001 conditions. Images representative of at least n = 3 per condition with two experimental repeats. Arrows show organoids with morphological changes. Bright field images. Scale bar represents 1250µm.

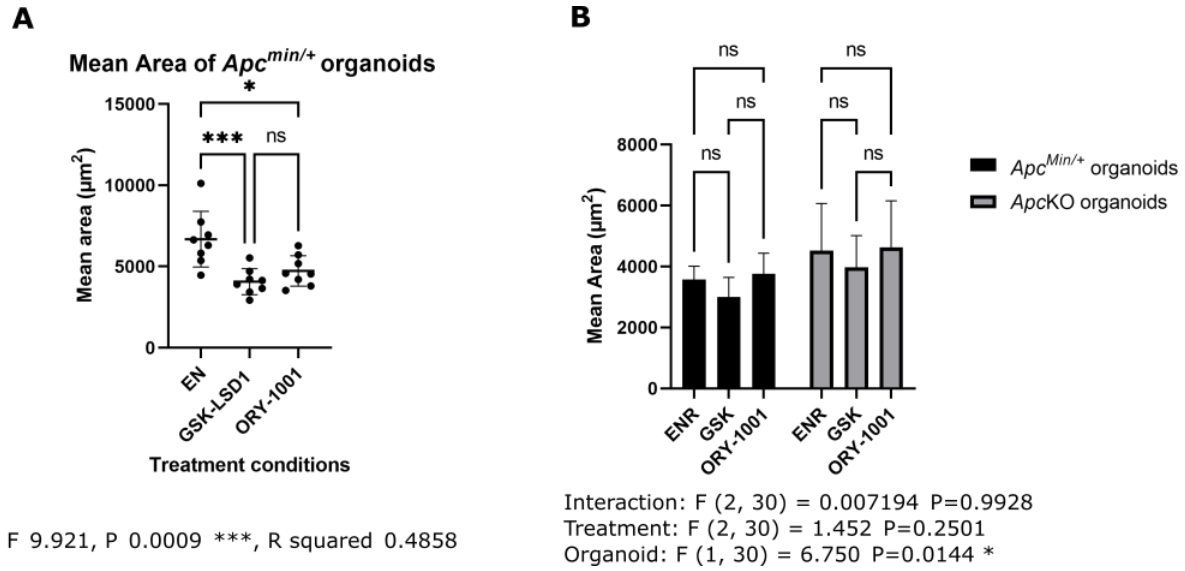

Figure 4-8: Mean area of *Apc*$^{Min/+}$ organoids showed significant reduction in size on LSD1 inhibition. (A) Graph representing mean area measurements from each well of *Apc*$^{Min/+}$ organoids: *n* = 8 per condition. Numerical data are means with 95% confidence intervals. Significant reduction in mean area between GSK-LSD1 treated organoids compared to the control organoids noted ***. Significant reduction in mean area between ORY-1001 and control organoids *. (B) Graph representing mean area measurements from *Apc*$^{Min/+}$ and *Apc*KO organoids, *n* = 6 for each condition and genotype. Numerical data are means ± SD. Significant source of variation in mean area from organoid type *, No significant differences noted between LSD1 inhibtor treated organoids compared to controls. (A) One -way ANOVA with Tukey's post hoc test and (B) Two-way ANOVA with Tukey's post hoc test was performed to determine significance. * P⩽ 0.05, ** P < 0.01, *** P ⩽ 0.001.

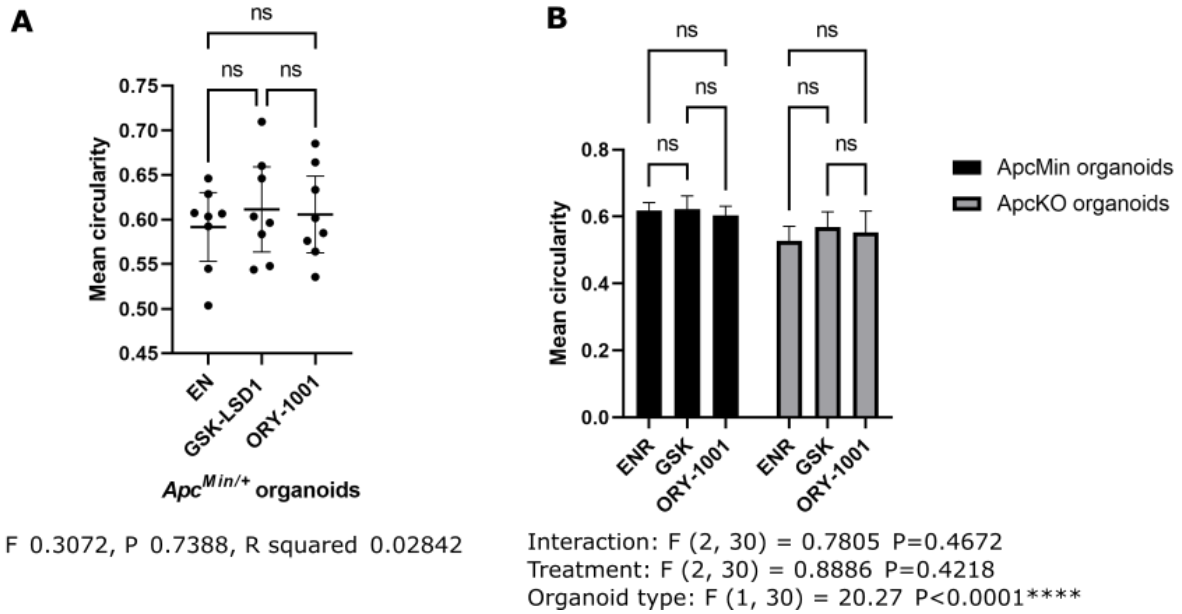

Figure 4-9: No significant differences in mean circularity were observed in *Apc*$^{Min/+}$ and *Apc*KO genotypes in LSD1 inhibiting conditions. (A) Graph represents mean circularity measurements of *Apc*$^{Min/+}$ organoids under control (EN), EN + GSK-LSD1, or EN + ORY-1001 conditions. *n* = 8 for each condition. Numerical data are means with 95% confidence intervals. No significant differences in mean circularity between LSD1 inhibitor treated organoids compared to the control organoids were noted. (B) Graph represents mean circularity measurements from *Apc*$^{Min/+}$ and *Apc*KO organoids under control (EN), EN + GSK-LSD1, or EN + ORY-1001 conditions. *n* = 6 for each condition and genotype. Numerical data are means ± SD. Organoid type contributed a significant source of variation in mean circularity ****. *Apc*KO organoids were less circular, but no other significant differences were noted between the treatment groups. (A) One - way ANOVA with Tukey's post hoc test and (B) Two-way ANOVA with Tukey's post hoc test was performed to determine significance. * P$\leqslant$ 0.05, ** P < 0.01, *** P $\leqslant$ 0.001.

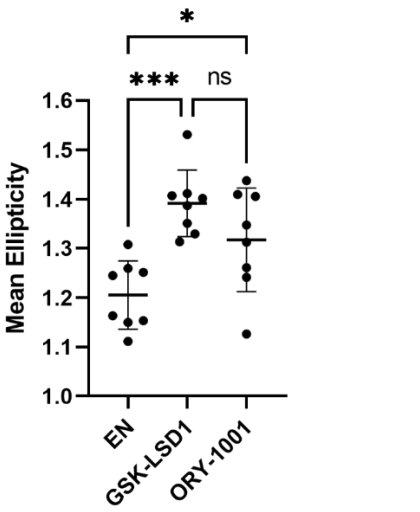

Figure 4-10: LSD1 inhibited *Apc$^{Min/+}$* organoids are significantly more elliptical than those grown in EN. Graph represents mean ellipticity measurements of *Apc$^{Min/+}$*organoids under control (EN), EN + GSK-LSD1, or EN + ORY-1001 conditions. *n* = 8 for each condition. Numerical data are means with SD. The major axis length (A) and minor axis lengths (B) of each organoid was measured and the ratio of (A/B) was calculated. A/B = 1 when an organoid was circular and was more elliptical when the ratio > 1. Means of this ratio was calculated for each well. One -way ANOVA with Tukey's post hoc test was performed to determine significance. * P$\leqslant$ 0.05, ** P < 0.01, *** P $\leqslant$ 0.001.

4.4 E-Cadherin is increased with a diffuse distribution in the cytoplasm of *Apc$^{Min/+}$* organoids on LSD1 inhibition.

The relationship between high LSD1 expression and an increased TNM staging in cancer has been discussed in section 1.5.2 E-cadherin suppression because of high LSD1 is a key factor in EMT (Jie et al., 2013). In addition, high LSD1 expression has been associated with higher LGR5 levels and LSD1 inhibition has been shown to result in WNT pathway inactivation (Hsu et al., 2015). To investigate the effects on E-cadherin and β-catenin in *Apc$^{Min/+}$* organoids under LSD1 inhibited conditions, *Apc$^{Min/+}$*organoids are grown in BCM-EN, BCM-EN with 5μm GSK LSD1 inhibitor and BCM-EN with 100nm ORY 1001 LSD1 inhibitor for 5 days and subsequently immunofluorescent stained for E-cadherin and β-catenin. Confocal microscopy images were taken and as seen in figure 4-11 the morphology of the cells within the organoid were better delineated as the cell membranes are visible through E-cadherin staining. LSD1 inhibited organoids had cells that were more varied in size and shape, with some larger cells on visual inspection (comparing images in figure 4-11D, E and F). E- cadherin is detected in stronger intensities in the cellular membranes of organoids in control (ENR) conditions. The fluorescent signal is more diffused, displaying greater presence of E-cadherin within the cytoplasm as well as the cellular membranes in LSD1 inhibitor treated organoids. In the control organoids β-catenin appears in the cellular membranes as well as the cytoplasm of some cells. β-catenin appears to be even more diffusedly distributed in LSD1 inhibited

organoids, with a greater proportion of the fluorescent signal seen in the cytoplasmic area of the cells.

Fluorescence intensities of these two proteins of interest was measured and as seen in figure 4-11M E-cadherin fluorescence intensity in increased in GSK-LSD1 treated organoids compared to both control and ORY-1001. Figure 4-11N shows that β-catenin fluorescence intensity is increased in GSK-LSD1 treated organoids compared to control.

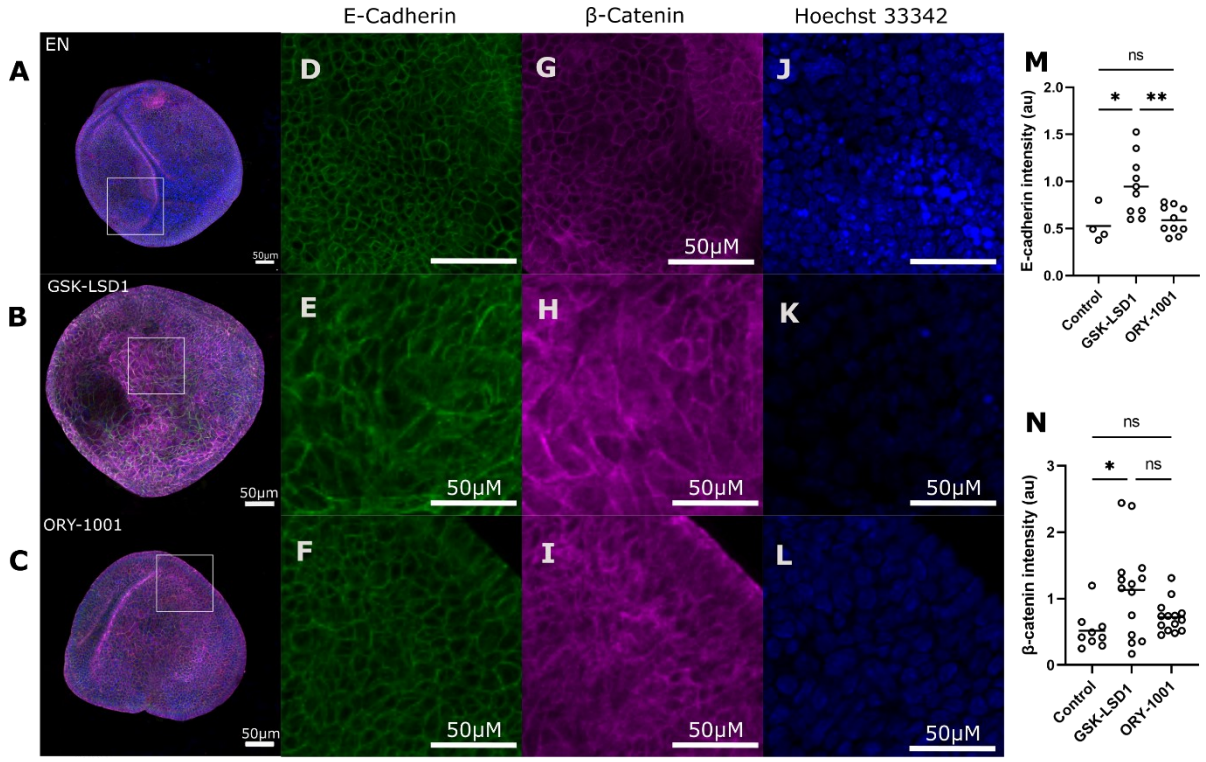

Figure 4-11: E-cadherin and β-catenin protein expression is increased in *Apc$^{Min/+}$* tumour organoids treated with GSK-LSD1 compared to control. Representative maximum intensity projections of confocal microscopy images of E-cadherin and β-catenin stained *Apc$^{Min/+}$* organoids. Scale bar represents 50μm for all images. Images are representative of at least n = 5 for organoids in control conditions and n = 10 per LSD1 inhibited condition. (A-C) Confocal image of immunofluorescent stained *Apc$^{Min/+}$* organoids in control (EN), GSK-LSD1 and ORY-1001 with all channels merged, E-cadherin, β-catenin, UEA1 and Hoechst 33342. (D-L) Magnified sections of insets showing distribution of E-cadherin (green), β-catenin (magenta) and Hoechst 33342 (blue). (D and E) Greater variation in size and shapes of cells within organoids treated with LSD1 inhibitor compared to control. (D-F) E-cadherin distribution more diffused and not confined to the membranes in GSK.LSD1 treated organoids compared to controls. (G-I) β-catenin more diffusely distributed in LSD1 inhibited organoids. (M) Graph represents fluorescence intensity of E-cadherin in organoids under control and LSD1 inhibited conditions. F=7.037, P 0.0046 ** R^2=0.4013, *n* = 4 for EN control, 10 for both GSK-LSD1 and ORY-1001 treated groups. Numerical data are means. (N) Graph represents fluorescence intensity of β-catenin in organoids under control and LSD1 treated conditions. F=5.084, P 0.0117 *, R^2= 0.2302, *n* = 9 for EN control, 14 for both GSK-LSD1 and ORY-1001 treated groups. Numerical data are means. (M, N) Intensities of protein of interest measured and normalized against Hoechst 33342 for each organoid. One-way ANOVA and Tukey's post-hoc tests were performed to determine significance. * P⩽ 0.05, ** P < 0.01, *** P ⩽ 0.001.

4.5 SOX9 intensities were similar between LSD1 inhibited organoids and controls.

As high levels of SOX9 expression in tumors with a constitutive activation of WNT signalling is a potential contributing factor in levels of tumor differentiation and cancer progression (Blache et al., 2004), the impact of LSD1 inhibition in *Apc*$^{Min/+}$ on SOX9 expression was of interest. This was investigated by growing *Apc*$^{Min/+}$ organoids in BCM-EN, BCM-EN with 5μm GSK LSD1 inhibitor and BCM-EN with 100nm ORY 1001 LSD1 inhibitor for 5 days and subsequently immunofluorescent stained for SOX9. Confocal microscopy images are shown in figure 4-12 where SOX9 staining follows a pattern of nuclear distribution in both treated and control organoids. There was no significant difference in SOX9 intensity between the treatment groups (figure 4-12G).

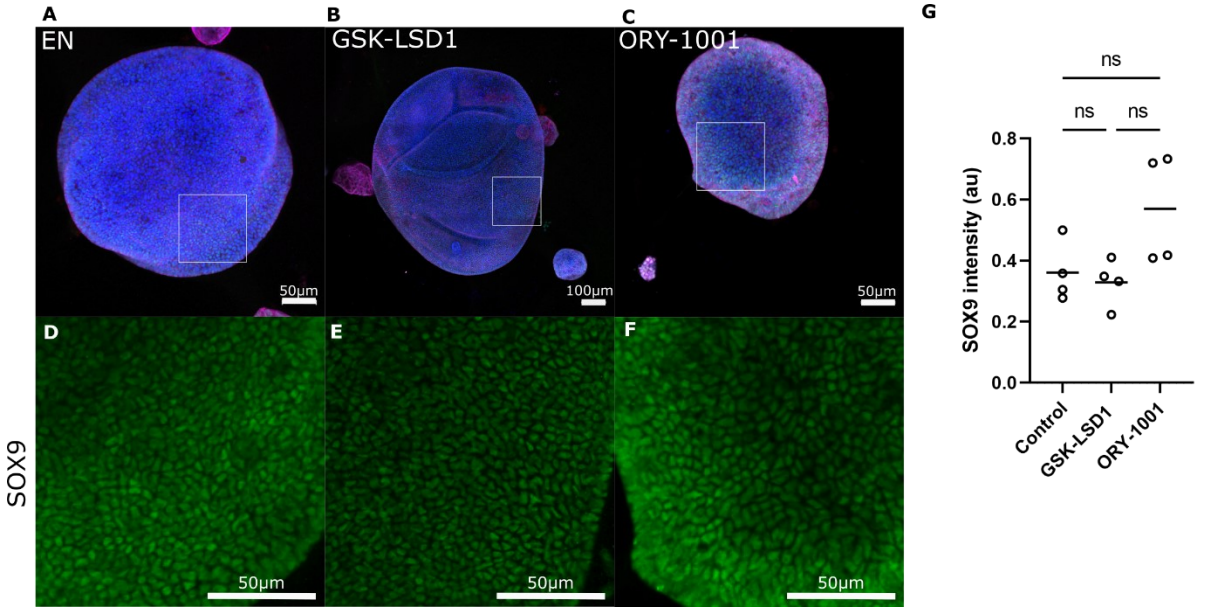

Figure 4-12: *Apc*$^{Min/+}$ organoids display no significant differences in SOX9 intensities and distribution between LSD1 inhibitor treated conditions and those in control.
Representative maximum intensity projections of confocal microscopy images of SOX9 stained *Apc*$^{Min/+}$ organoids. Images representative of n = 4 organoids per condition. (A – C) Immunofluorescent staining of *Apc*$^{Min/+}$ organoids in control (EN), GSK-LSD1 and ORY-1001 with all channels merged, SOX9 (green), β-catenin (magenta), UEA1 (red) and Hoechst 33342 (blue). (D-F) Magnified section showing staining for SOX9 has a nuclear distribution. (G) Graph represents fluorescence intensity of SOX9 in organoids treated in control and LSD1 inhibited conditions. F=4.248, P 0.0502, R^2=0.4856, *n* = 4 for all conditions. Numerical data are means. Intensities of SOX9 measured and normalized against Hoechst 33342 for each organoid. One-way ANOVA and Tukey's post-hoc tests were performed to determine significance. * P⩽ 0.05, ** P < 0.01, *** P ⩽ 0.001.

4.6 Increase in Filamin A on LSD1 inhibition of *Apc*$^{Min/+}$ and *Apc*KO organoids

The literature shows that genes associated with cytoskeletal organization such as *Flna* were upregulated in LSD1 depleted states (N. Parmar et al., 2021). An increase in FLNA protein levels in LSD1 KO organoids and LSD1 inhibited organoids has also been demonstrated (N. Parmar et al., 2021; Zwiggelaar et al., 2020).

We postulate that elements of cytoskeletal organization such a FLNA and F actin are likely to be increased in LSD1 inhibited *Apc*$^{Min/+}$ and *Apc*KO organoids as well. Thus, *Apc*$^{Min/+}$ and *Apc*KO organoids were grown in BCM-EN, BCM-EN with 5μm GSK LSD1 inhibitor and BCM-EN with 100nm ORY 1001 LSD1 inhibitor for 4 days. The organoids were subsequently stained for FLNA, F actin, β-catenin, and Hoechst 3342.
On visual inspection of organoids FLNA fluorescence signal intensity for LSD1 inhibited *Apc*$^{Min/+}$ and *Apc*KO organoids was increased compared to untreated organoids while F actin distribution and intensity appeared similar in all treatment groups for both genotypes. β-catenin distribution is more diffused and signal intensity increased in LSD1 inhibitor treated groups (figures 4-13 and 4-14)

A significant increase in measured intensity of FLNA was seen in *Apc*KO organoids treated with GSK-LSD1 (figure 4-15A). No significant difference in F actin was observed in all conditions for both genotypes (figure 4-15B). β-catenin was significantly higher in GSK-LSD1 compared to ORY-1001 treated *Apc*KO organoid, however no significant differences were seen in its intensity among other treatment conditions.

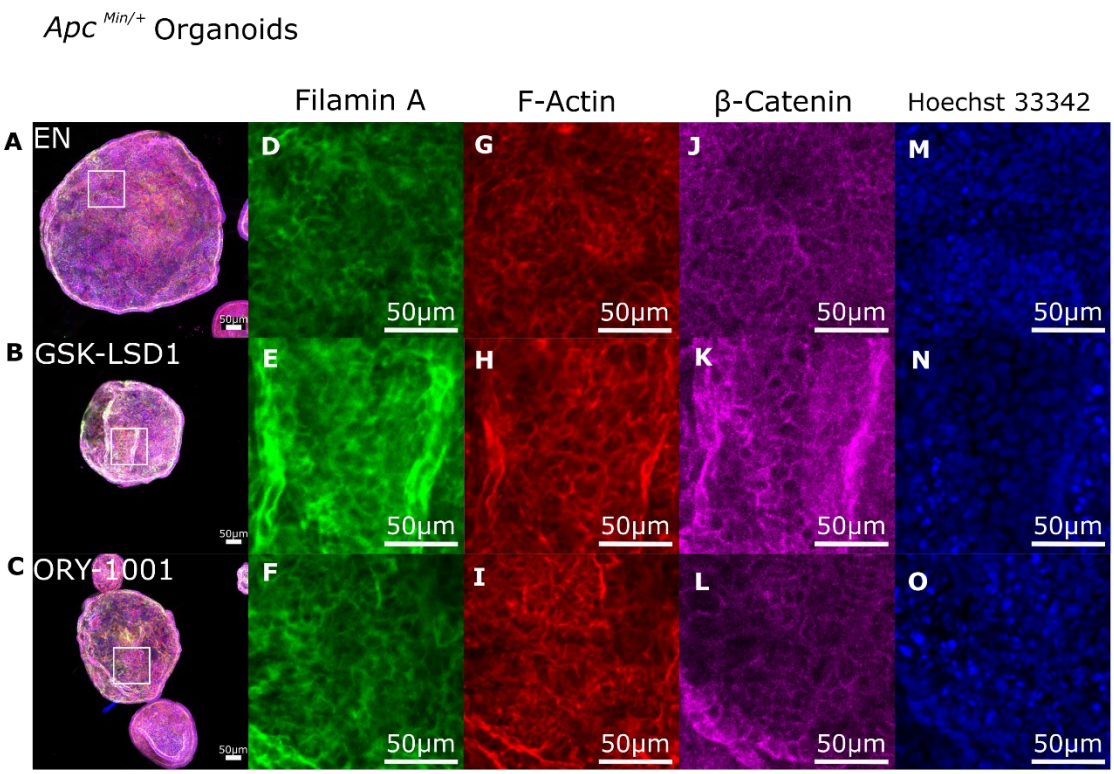

Figure 4-13: *Apc*$^{Min/+}$ organoids show an increased distribution and intensity of FLNA in LSD1 inhibited conditions. Representative maximum intensity projections of confocal microscopy images of *Apc*$^{Min/+}$ organoids. Images representative of at least n = 9 per condition. (A-C) Confocal images of immunofluorescence stained *Apc*$^{Min/+}$ organoids under control (EN), GSK-LSD1 and ORY-1001 conditions with all channels merged, FLNA, F actin, β-catenin and Hoechst 33342. (D-O) Magnified images of insets showing distribution and intensity of FLNA (green), F actin (red), β-catenin (magenta) and Hoechst 33342 (blue). (E, F) Increase fluorescence signal intensity for FLNA in GSK-LSD1 and ORY-1001 treated organoids compared to (D) control. (G-I) F actin distribution and intensity similar among all groups. (K-L) β-catenin a more diffused distribution and increased intensity in GSK-LSD1 and ORY-1001 conditions.

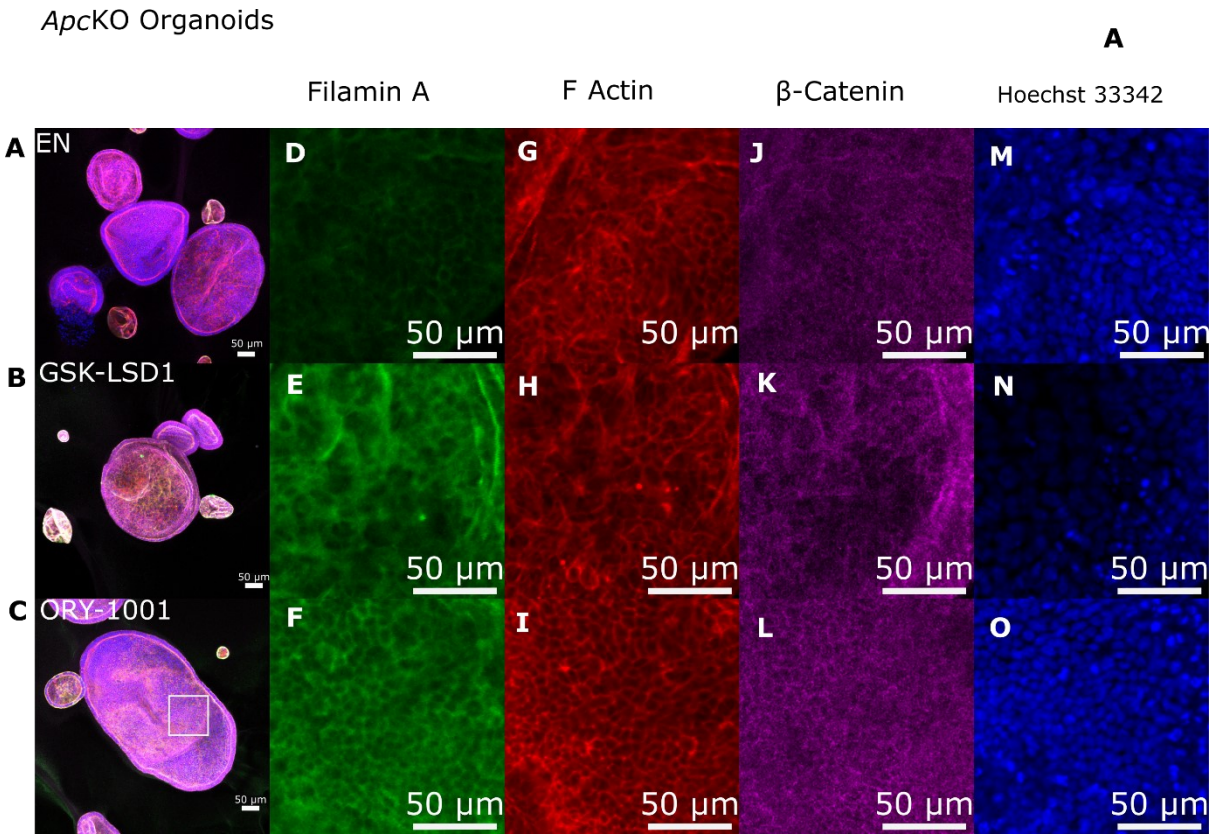

Figure 4-14: *Apc*KO organoids display an increased distribution and intensity of FLNA in LSD1 inhibited conditions. Representative maximum intensity projections of confocal microscopy images of FLNA, F actin and β-catenin stained *Apc*KO organoids. Image representative of at least n = 10 per condition. Scale bar represents 50µm. (A-C) Organoids under control (EN), GSK-LSD1 and ORY-1001 conditions with all channels merged, FLNA, F actin, β-catenin and Hoechst 33342. (D-O) Magnified images of insets showing distribution and intensity of FLNA (green), F actin (red), β-catenin (magenta) and Hoechst 33342 (blue). (E, F) Increase fluorescence signal intensity in GSK-LSD1 and ORY-1001 treated organoids compared to (D) control. (G-I) F actin distribution and intensity similar among all groups. (K-L) β-catenin a more diffused distribution and increased intensity in GSK-LSD1 and ORY-1001 conditions.

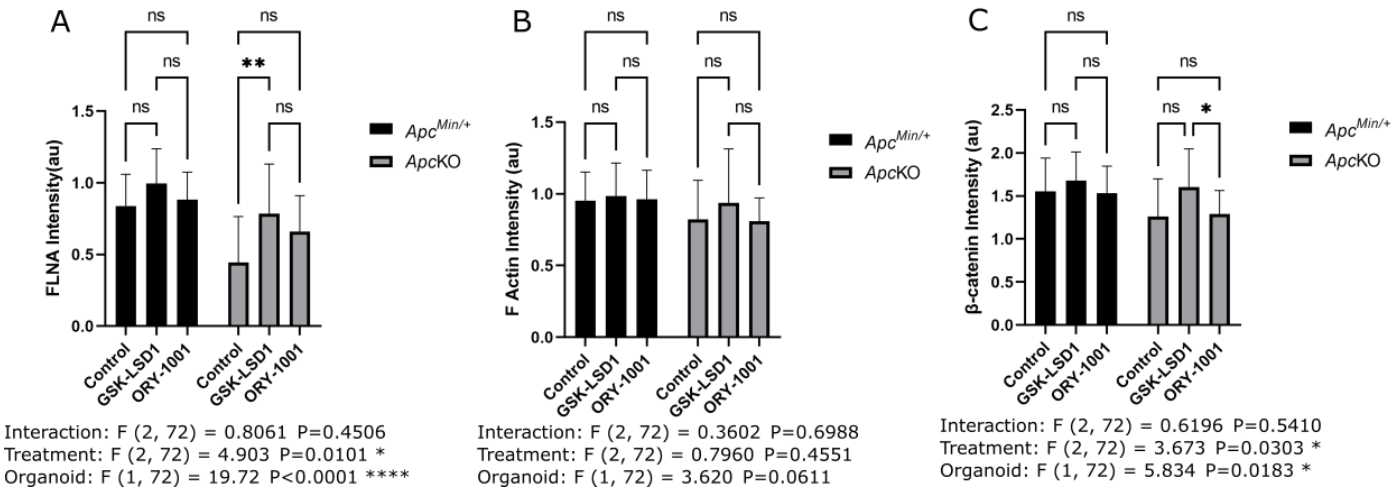

Figure 4-15: Increased fluorescence signal intensity for FLNA for ApcKO organoids in GSK-LSD1 conditions compared to control. *(A*, B and C*)* Graph represents intensity of FLNA (A), F actin (B) and β-catenin (C) for *Apc*$^{Min/+}$ and *Apc*KO organoids under LSD1 inhibited and control conditions. Control, EN (without RSPO), EN + 5μm GSK-LSD1 or EN + 100nm ORY-1001. Intensities of each target protein was measured and normalised against the intensity of Hoechst 33342 for each organoid. For all graphs n = 9 (EN), 13 (GSK-LSD1) and 15 (ORY-1001) for *Apc*$^{Min/+}$ organoids and n = 10 (EN), 15 (GSK-LSD1) and 16 (ORY-1001) for *Apc*KO organoids. Numerical data are means ± SD. (A) Significant difference in intensity of FLNA in GSK-LSD1 treated *Apc*KO organoids compared to control **. (B) No significant difference in intensities of F actin observed in all conditions and both groups. (C) Significant difference in intensity of β-catenin in GSK-LSD1 treated *Apc*KO organoids compared to ORY-1001 treated *. Two-way ANOVA and Tukey's post-hoc tests were performed to determine significance. * P$\leqslant$ 0.05, ** P < 0.01, *** P $\leqslant$ 0.001.

4.7 Raised β-catenin levels on LSD1 inhibition of *Apc*$^{Min/+}$ organoids.

Organoids grown in WNT enhanced conditions, are likely to have greater activation of WNT pathway signalling and hence have higher β-catenin levels. However, LSD1 inhibition has been shown to downregulate LGR5 and lead to the inactivation of the WNT/ β-catenin pathway (Hsu et al., 2015). This would suggest that a LSD1 KO organoid would have lower β-catenin levels compared to a LSD1 WT when exposed to WNT.

To study this, LSD1 WT and LSD1 KO organoids were grown for 4 days in BCM-ENR, BCM-ENR + WNT3a 25% and BCM-ENR + CHIR 99021 3μm, protein lysates were extracted at 24H and 96H time points. Western blots were run, intensities measures and analysed as seen in figure 4-16. Here a significant decrease in β-catenin is seen between LSD1 WT organoids and LSD1 KO organoids exposed to WNT3a (figure 4-16B)

In *Apc*$^{Min/+}$ and *Apc*KO organoids which has a constitutive activation of the WNT pathway, it can be anticipated that LSD1 inhibition is likely to have less impact on β-catenin levels. To test this *Apc*$^{Min/+}$ and *Apc*KO were grown in BCM-EN, BCM-EN with 5μm GSK LSD1 inhibitor and BCM-EN with 100nm ORY 1001 LSD1 and protein lysates extracted on day

5. Western blots were run, intensities measured and analysed as in figure 4-17. No significant differences were noted between the treatment groups of both genotypes.

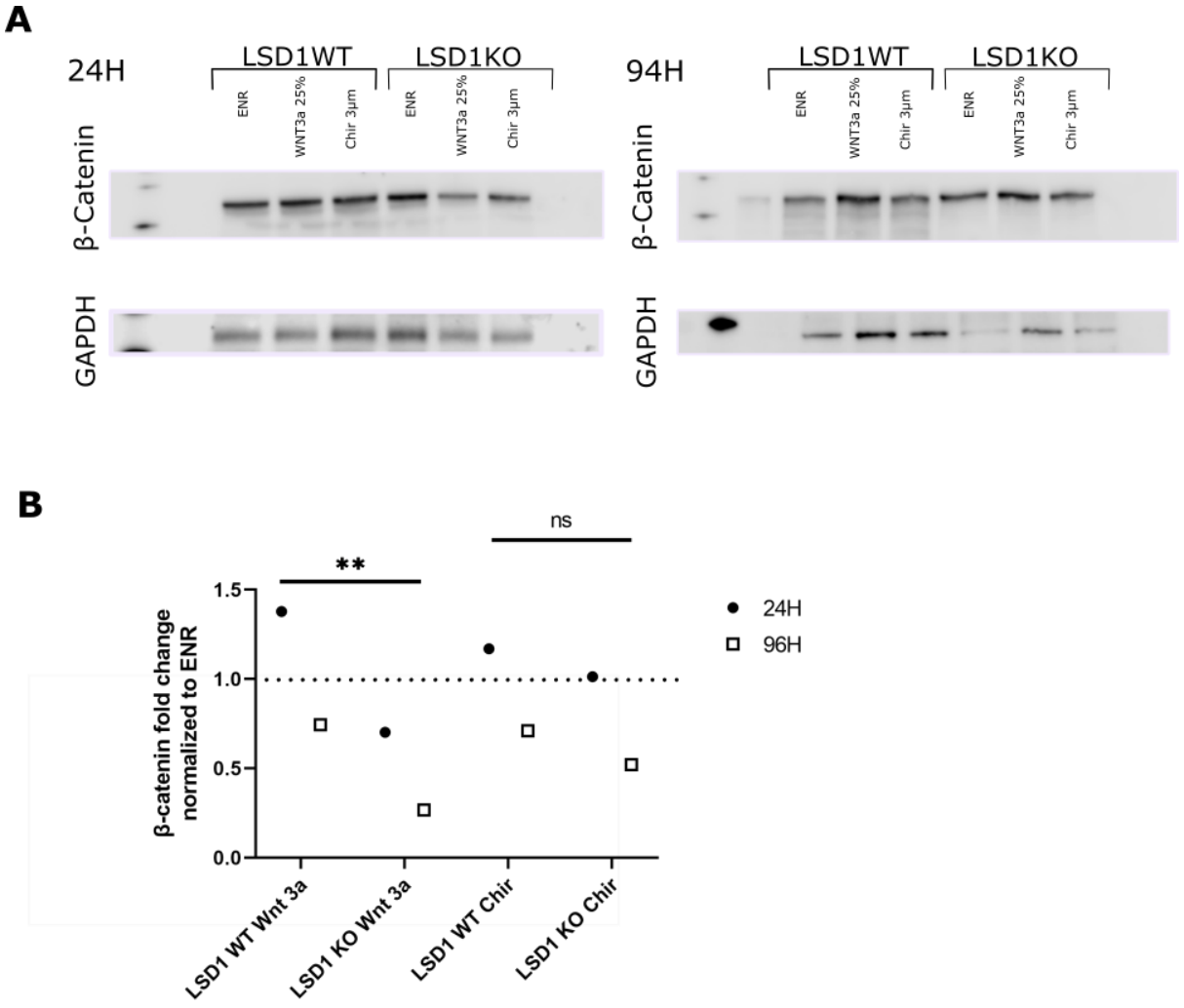

Figure 4-16: A significant decrease in fold change of β-catenin levels is seen between LSD1 WT and LSD1 KO in WNT3a enhanced condition. (A) Western blots β-catenin of LSD1 WT and LSD1 KO under WNT enhanced conditions after 24H and 96H. Control media ENR, ENR + WNT3a 25% or ENR + CHIR99021 3µm. GAPDH used as housekeeping gene (B) Graph representing β-catenin fold change normalized to ENR of LSD1 WT and LSD1 KO under WNT enhanced conditions. Duration of exposure to WNT ** and type of organoid and treatment ** were significant sources of variation. A significant decrease in fold change of β-catenin levels is seen between LSD1 WT and LSD1 KO in WNT3a enhanced condition **. For each time point n = 6. Two-way ANOVA and Tukey's post-hoc tests were performed to determine significance. * P$\leqslant$ 0.05, ** P < 0.01, *** P $\leqslant$ 0.001.

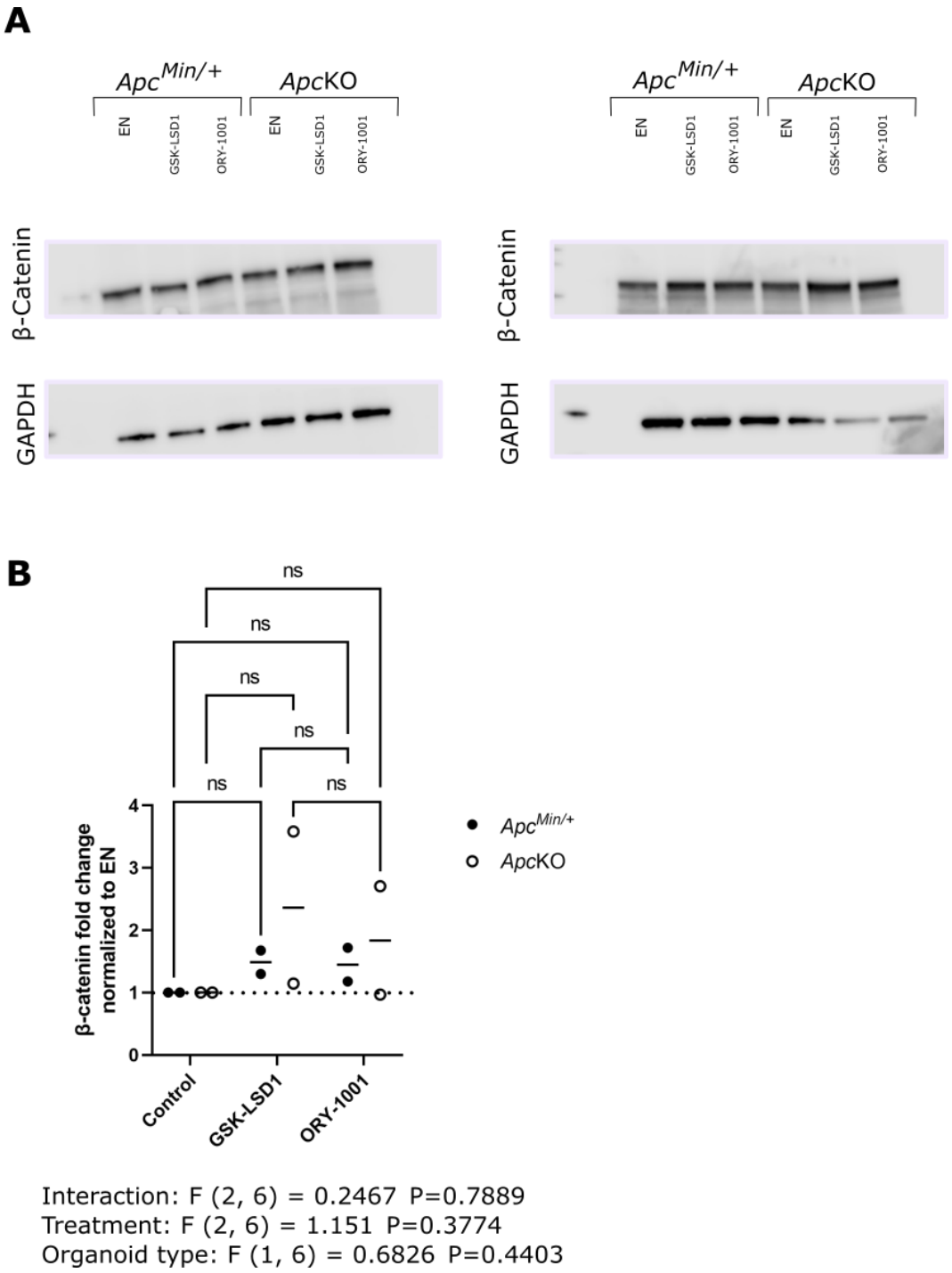

Figure 4-17: No significant differences in fold change of β-catenin between treatment conditions in *Apc*$^{Min/+}$ and *Apc*KO organoids. (A) Western blots for β-catenin levels of *Apc*$^{Min/+}$and *Apc*KO organoids grown in EN, EN + 5μm GSK-LSD1 or EN + 100nm ORY-1001 conditions for 5 days. GAPDH used as housekeeping gene. (B) Graph represents β-catenin fold change normalized to EN of *Apc*$^{Min/+}$and *Apc*KO organoids grown under LSD1 inhibitory conditions. No significant differences in fold change for β-catenin between all treatment conditions and genotypes. Each dot represents fold change of β-catenin normalized to ENR which is derived from measured band intensities of β-catenin on western blot normalized against the band intensity of housekeeping gene GAPDH. n = 2 for each of the conditions, per genotype. Two-way ANOVA and Tukey's post-hoc tests were performed to determine significance. * P⩽ 0.05, ** P < 0.01, *** P ⩽ 0.001

5 Discussion

We first characterised how normal intestinal organoids and LSD1 KO organoids responded to increased WNT exposure. LSD1 KO organoids appeared to maintain its ability to form crypts despite the increased activation of the WNT pathway compared to LSD1 WT organoids that became enlarged and spherical. Earlier studies carried out by Zwiggelaar et al on the impact of LSD1 depletion in intestinal epithelium has shown an expansion of the ISC population and almost complete loss of Paneth cells. Despite the loss of Paneth cells, LSD1 KO organoids grew successfully without external WNT supplementation and continued to form crypts. In addition, blockade of WNT with IWP-2 in LSD1 KO organoids sustained growth. Hence it has been compared to the fetal spheroid in its ability to sustain growth without WNT supplementation but has a more mature morphology. Based on this, our findings of LSD1 KO organoids retaining a crypt forming morphology is as anticipated.

To investigate the role of LSD1 in WNT driven tumors, we used a mouse *Apc*$^{Min/+}$ and *Apc*KO intestinal organoid model as these display constitutive WNT signalling. On LSD1 inhibition a trend towards a more ellipsoid morphology with dimpling around the edges was apparent. *Apc*$^{Min/+}$organoids treated with LSD1 inhibitors were significantly more elliptical supporting our findings of a more ellipsoid morphology visually. Mean area calculation in initial *Apc*$^{Min/+}$organoids showed significant shrinking in size. However, on repeat experiments with both *Apc*$^{Min/+}$ and *Apc*KO no significant reduction in growth was noted. Though it was not significant, a slight trend of GSK-LSD1 organoids to be smaller than control organoids were noted. LSD1 has been identified as a therapeutic target of interest in cancer. For example, studies of leukemic and glioblastoma stem cells indicate that LSD1 maintains CSCs in an undifferentiated, therapy resistant state. Also, LSD1 inhibition has been shown to reduce tumorigenicity in breast, leukemic and glioblastoma CSCs and sensitizes hepatocellular CSCs to treatment (Karakaidos et al., 2019). This would suggest that LSD1 inhibition of tumor organoids could result in changes favourable to cancer treatment.

To assess the impact on the WNT signalling pathway, we looked at β-catenin expression and its downstream factor SOX9. Our results, show a significant increase in β-catenin in GSK-LSD1 treated *Apc*$^{Min/+}$ organoids and a trend towards an increase in β-catenin in the second set of experiments with *Apc*$^{Min/+}$ and *Apc*KO though results were not significant. Staining of β-catenin showed an increased distribution in the cytoplasm compared to the membranes in *Apc*$^{Min/+}$ organoids. SOX9 expression was similar in LSD1 inhibited and control groups in *Apc*$^{Min/+}$organoids. Due to the nature of the Apc mutation, the destruction complex of the WNT signalling pathway is disabled and β-catenin is anticipated to accumulate and translocate to the nucleus. Hence, despite LSD1 inhibition potentially down-regulating LGR5 in these organoids, little impact is expected in the overall β-catenin levels. Whether β-catenin expression is unaffected or increased in our study is inconclusive though they show a trend towards increased cytoplasmic β-catenin on LSD1 inhibition in *Apc*$^{Min/+}$organoids.

Our results show, an increase in E-cadherin intensities as well as a more diffuse distribution of E-cadherin in GSK-LSD1 and ORY-1001 inhibited *Apc*$^{Min/+}$ organoids. A

high LSD1 expression is associated with suppression of E-cadherin and so we postulate that LSD1 inhibition will reverse this. However, in normal healthy epithelium E-cadherin distribution is constrained to the membranes. Our study shows that LSD1 inhibition in *Apc*$^{Min/+}$ led to an increase in expression as well as a cytoplasmic distribution of E-cadherin. An increased expression and cytoplasmic localization of E-cadherin has been associated with adenomas in FAP (El-Bahrawy et al., 2002), and a worse prognosis in CRC and other human cancers (Bendardaf et al., 2019; Salon et al., 2005; Wijnhoven et al., 2002). Our result of an increase in E-cadherin expression indicates that E-cadherin suppression is reduced, however the increased cytoplasmic distribution might point to other interactions with the WNT signalling pathway. Therefore, it is inconclusive if LSD1 inhibition in *Apc*$^{Min/+}$ leads to a positive outcome in terms of inducing changes that would make a tumor more favourable to treatment.

Our research group has previously demonstrated that genes associated with cytoskeletal organization such as *Flna* were upregulated in LSD1 depleted states and that FLNA protein levels in LSD1 KO organoids and LSD1 inhibited organoids were increased (N. Parmar et al., 2021; Zwiggelaar et al., 2020). In our experiments, a trend of increased FLNA intensities was seen on LSD1 inhibition, with a significant increase of FLNA noted in *Apc*KO organoids treated with GSK-LSD1. In F actin, no significant differences were demonstrated between LSD1 treated groups and controls. FLNA impacts the actin network of cells by crosslinking actin filaments and hence, changing its rigidity. Our results indicate that F actin itself remains unchanged while FLNA expression is increased.

This study is largely based on organoid cultures and histological techniques. Organoid cultures provide a model in which various factors can be changed and outcomes measured in a timelier manner than in vivo studies. However, this method can result in variability between cultures due to differences in organoid seeding sizes and numbers between wells. To counter this variability a larger sample size and experimental repeats are required which takes time. Hence, organoid cultures are useful as a testing ground to discover the potential impact different factors may contribute but results would require further corroboration through *in vivo* experiments. Certain precautions were taken to reduce variability with organoid cultures, for each treatment condition and control, at least 3 wells were grown, and multiple experimental repeats were done. Live imaging of organoids was standardized using a standard protocol between days 1, 3 and 4 or 5 and the same script used to analyse measurements.

Immunostaining methods are useful as they provide a clear visible picture of structures and using different staining methods the chemistry of the tissues examined. Unfortunately, human error during the preparation and analysis of slides is possible. Hence, a limitation of this study is the lack of negative controls in IF imaging of organoids to account for non-specific binding of the secondary antibodies. However, these stainings have been previously performed in our research group and negative controls have been conducted for each primary antibody previously. The main limitation of this study is insufficient time as experimental repeats of organoid cultures are time consuming. Under optimal circumstances, more repeats of experiments with an increased sample size would be done and in the case of the subtle morphological changes seen in *Apc*$^{Min/+}$ on LSD1 inhibition, a further analysis of the mean ellipticity was carried out for the *Apc*$^{Min/+}$ organoids supporting our visual findings of a more elliptical morphology. Ideally the analysis would be carried out for the *Apc*$^{Min/+}$ and *Apc*KO organoid experiments as well if not for time constraints.

6 Conclusion

In this study we demonstrate that LSD1 inhibition in a WNT driven tumor model leads to an increased expression of FLNA and morphological changes (ellipsoid shape and dimpling along the edges) indicating changes in the cytoskeletal structure. These changes in morphology and cytoskeletal structure could potentially have an impact on tumor survival and sensitivity to treatment. Our results are inconclusive regarding the size of LSD1 inhibited organoids. We also show an increase in E-cadherin expression in GSK-LSD1 treated $Apc^{Min/+}$ organoids but not in ORY-1001 treated organoids. IF staining of $Apc^{Min/+}$ organoids show an increased cytoplasmic distribution of E-cadherin in LSD1 inhibited organoids. However, this data must be further validated. Further *in vivo* experiments are necessary to determine if there is a reduction in size of LSD1 depleted WNT driven tumors, and if the morphological changes we have seen are indicative of a decrease in characteristics favourable to tumor survival. It would be beneficial to quantify the expression and distribution of E-cadherin, β-catenin and FLNA upon LSD1 depletion *in vivo* to confirm the trends we see in this study.

References

Alegría-Torres, J. A., Baccarelli, A., & Bollati, V. (2011). Epigenetics and lifestyle. *Epigenomics*, *3*(3), 267-277. https://doi.org/10.2217/epi.11.22

Audia, J. E., & Campbell, R. M. (2016). Histone Modifications and Cancer. *Cold Spring Harbor Perspectives in Biology*, *8*(4), a019521. https://doi.org/10.1101/cshperspect.a019521

Barker, N., Ridgway, R. A., van Es, J. H., van de Wetering, M., Begthel, H., van den Born, M., Danenberg, E., Clarke, A. R., Sansom, O. J., & Clevers, H. (2009). Crypt stem cells as the cells-of-origin of intestinal cancer. *Nature*, *457*(7229), 608-611. https://doi.org/10.1038/nature07602

Barker, N., van Es, J. H., Kuipers, J., Kujala, P., van den Born, M., Cozijnsen, M., Haegebarth, A., Korving, J., Begthel, H., Peters, P. J., & Clevers, H. (2007). Identification of stem cells in small intestine and colon by marker gene Lgr5. *Nature*, *449*(7165), 1003-1007. https://doi.org/10.1038/nature06196

Baron, R., Binda, C., Tortorici, M., McCammon, J. A., & Mattevi, A. (2011). Molecular mimicry and ligand recognition in binding and catalysis by the histone demethylase LSD1-CoREST complex. *Structure*, *19*(2), 212-220. https://doi.org/10.1016/j.str.2011.01.001

Basak, O., Beumer, J., Wiebrands, K., Seno, H., Van Oudenaarden, A., & Clevers, H. (2017). Induced Quiescence of Lgr5+ Stem Cells in Intestinal Organoids Enables Differentiation of Hormone-Producing Enteroendocrine Cells. *Cell Stem Cell*, *20*(2), 177-190.e174. https://doi.org/10.1016/j.stem.2016.11.001

Baylin, S. B., & Jones, P. A. (2016). Epigenetic Determinants of Cancer. *Cold Spring Harbor Perspectives in Biology*, *8*(9), a019505. https://doi.org/10.1101/cshperspect.a019505

Bendardaf, R., Sharif-Askari, F. S., Sharif-Askari, N. S., Syrjänen, K., & Pyrhönen, S. (2019). Cytoplasmic E-Cadherin Expression Is Associated With Higher Tumour Level of VEGFA, Lower Response Rate to Irinotecan-based Treatment and Poorer Prognosis in Patients With Metastatic Colorectal Cancer. *Anticancer Res*, *39*(4), 1953-1957. https://doi.org/10.21873/anticanres.13305

Bienz, M., & Clevers, H. (2000). Linking Colorectal Cancer to Wnt Signaling. *Cell*, *103*(2), 311-320. https://doi.org/10.1016/s0092-8674(00)00122-7

Blache, P., Van De Wetering, M., Duluc, I., Domon, C., Berta, P., Freund, J.-N. L., Clevers, H., & Jay, P. (2004). SOX9 is an intestine crypt transcription factor, is regulated by the Wnt pathway, and represses the CDX2 and MUC2 genes. *Journal of Cell Biology*, *166*(1), 37-47. https://doi.org/10.1083/jcb.200311021

Boyer, B., Vallés, A. M., & Edme, N. (2000). Induction and regulation of epithelial-mesenchymal transitions. *Biochem Pharmacol*, *60*(8), 1091-1099. https://doi.org/10.1016/s0006-2952(00)00427-5

Bray, F., Ferlay, J., Soerjomataram, I., Siegel, R. L., Torre, L. A., & Jemal, A. (2018). Global cancer statistics 2018: GLOBOCAN estimates of incidence and mortality worldwide for 36 cancers in 185 countries. *CA: A Cancer Journal for Clinicians*, *68*(6), 394-424. https://doi.org/10.3322/caac.21492

Breault, D. T., Min, I. M., Carlone, D. L., Farilla, L. G., Ambruzs, D. M., Henderson, D. E., Algra, S., Montgomery, R. K., Wagers, A. J., & Hole, N. (2008). Generation of mTert-GFP mice as a model to identify and study tissue progenitor cells. *Proceedings of the National Academy of Sciences*, *105*(30), 10420-10425. https://doi.org/10.1073/pnas.0804800105

Cao, J. (2014). The functional role of long non-coding RNAs and epigenetics. *Biological Procedures Online*, *16*(1), 11. https://doi.org/10.1186/1480-9222-16-11

Chen, T., You, Y., Jiang, H., & Wang, Z. Z. (2017). Epithelial-mesenchymal transition (EMT): A biological process in the development, stem cell differentiation, and tumorigenesis. *J Cell Physiol*, *232*(12), 3261-3272. https://doi.org/10.1002/jcp.25797

Cheng, H., & Leblond, C. P. (1974). Origin, differentiation and renewal of the four main epithelial cell types in the mouse small intestine. V. Unitarian Theory of the origin of the four epithelial cell types. *Am J Anat*, *141*(4), 537-561. https://doi.org/10.1002/aja.1001410407

Cho, H.-S., Suzuki, T., Dohmae, N., Hayami, S., Unoki, M., Yoshimatsu, M., Toyokawa, G., Takawa, M., Chen, T., Kurash, J. K., Field, H. I., Ponder, B. A. J., Nakamura, Y., & Hamamoto, R. (2011). Demethylation of RB Regulator MYPT1 by Histone Demethylase LSD1 Promotes Cell Cycle Progression in Cancer Cells. *Cancer Research*, *71*(3), 655-660. https://doi.org/10.1158/0008-5472.can-10-2446

Cook, D. J. a. W., P.J. (2015). *Cellular Pathology; An Introduction to Techniques and Applications* (Third edition ed.). Scion Publishing.

Darwich, A. S., Aslam, U., Ashcroft, D. M., & Rostami-Hodjegan, A. (2014). Meta-analysis of the turnover of intestinal epithelia in preclinical animal species and humans. *Drug Metab Dispos*, *42*(12), 2016-2022. https://doi.org/10.1124/dmd.114.058404

De Lau, W., Peng, W. C., Gros, P., & Clevers, H. (2014). The R-spondin/Lgr5/Rnf43 module: regulator of Wnt signal strength. *Genes & Development*, *28*(4), 305-316. https://doi.org/10.1101/gad.235473.113

Ding, J., Zhang, Z. M., Xia, Y., Liao, G. Q., Pan, Y., Liu, S., Zhang, Y., & Yan, Z. S. (2013). LSD1-mediated epigenetic modification contributes to proliferation and metastasis of colon cancer. *Br J Cancer*, *109*(4), 994-1003. https://doi.org/10.1038/bjc.2013.364

Dupont, C., Armant, D., & Brenner, C. (2009). Epigenetics: Definition, Mechanisms and Clinical Perspective. *Seminars in Reproductive Medicine*, *27*(05), 351-357. https://doi.org/10.1055/s-0029-1237423

Durand, A., Donahue, B., Peignon, G., Letourneur, F., Cagnard, N., Slomianny, C., Perret, C., Shroyer, N. F., & Romagnolo, B. (2012). Functional intestinal stem cells after Paneth cell ablation induced by the loss of transcription factor Math1 (Atoh1). *Proc Natl Acad Sci U S A*, *109*(23), 8965-8970. https://doi.org/10.1073/pnas.1201652109

Ee, H. C., Erler, T., Bhathal, P. S., Young, G. P., & James, R. J. (1995). Cdx-2 homeodomain protein expression in human and rat colorectal adenoma and carcinoma. *Am J Pathol*, *147*(3), 586-592.

El-Bahrawy, M. A., Talbot, I. C., Poulsom, R., Jeffery, R., & Alison, M. R. (2002). The expression of E-cadherin and catenins in colorectal tumours from familial adenomatous polyposis patients. *The Journal of Pathology*, *198*(1), 69-76. https://doi.org/10.1002/path.1168

Farin, H. F., Van Es, J. H., & Clevers, H. (2012). Redundant sources of Wnt regulate intestinal stem cells and promote formation of Paneth cells. *Gastroenterology*, *143*(6), 1518-1529.e1517. https://doi.org/10.1053/j.gastro.2012.08.031

Fearon, E. R. (1991). A genetic basis for the multi-step pathway of colorectal tumorigenesis. *Princess Takamatsu Symp*, *22*, 37-48.

Ferrari-Amorotti, G., Fragliasso, V., Esteki, R., Prudente, Z., Soliera, A. R., Cattelani, S., Manzotti, G., Grisendi, G., Dominici, M., Pieraccioli, M., Raschellà, G., Chiodoni, C., Colombo, M. P., & Calabretta, B. (2013). Inhibiting Interactions of Lysine Demethylase LSD1 with Snail/Slug Blocks Cancer Cell Invasion. *Cancer Research*, *73*(1), 235-245. https://doi.org/10.1158/0008-5472.can-12-1739

Gehart, H., & Clevers, H. (2019). Tales from the crypt: new insights into intestinal stem cells. *Nature Reviews Gastroenterology & Hepatology*, *16*(1), 19-34. https://doi.org/10.1038/s41575-018-0081-y

Greer, E. L., & Shi, Y. (2012). Histone methylation: a dynamic mark in health, disease and inheritance. *Nat Rev Genet*, *13*(5), 343-357. https://doi.org/10.1038/nrg3173

Grün, D., Lyubimova, A., Kester, L., Wiebrands, K., Basak, O., Sasaki, N., Clevers, H., & Van Oudenaarden, A. (2015). Single-cell messenger RNA sequencing reveals rare intestinal cell types. *Nature*, *525*(7568), 251-255. https://doi.org/10.1038/nature14966

Gu, L., Cong, J., Zhang, J., Tian, Y. Y., & Zhai, X. Y. (2016). A microwave antigen retrieval method using two heating steps for enhanced immunostaining on aldehyde-fixed paraffin-embedded tissue sections. *Histochem Cell Biol*, *145*(6), 675-680. https://doi.org/10.1007/s00418-016-1426-7

Gumbiner, B. M., & McCrea, P. D. (1993). Catenins as mediators of the cytoplasmic functions of cadherins. *Journal of Cell Science*, *1993*(Supplement_17), 155-158. https://doi.org/10.1242/jcs.1993.supplement_17.22

Half, E., Bercovich, D., & Rozen, P. (2009). Familial adenomatous polyposis. *Orphanet J Rare Dis*, *4*, 22. https://doi.org/10.1186/1750-1172-4-22

Hanahan, D., & Robert. (2011). Hallmarks of Cancer: The Next Generation. *Cell*, *144*(5), 646-674. https://doi.org/10.1016/j.cell.2011.02.013

Helander, H. F., & Fändriks, L. (2014). Surface area of the digestive tract - revisited. *Scand J Gastroenterol*, *49*(6), 681-689. https://doi.org/10.3109/00365521.2014.898326

Hinoi, T., Loda, M., & Fearon, E. R. (2003). Silencing of CDX2 expression in colon cancer via a dominant repression pathway. *J Biol Chem*, *278*(45), 44608-44616. https://doi.org/10.1074/jbc.M307435200

Hnasko, T. S., & Hnasko, R. M. (2015). The Western Blot. *Methods Mol Biol*, *1318*, 87-96. https://doi.org/10.1007/978-1-4939-2742-5_9

Hsu, H. C., Liu, Y. S., Tseng, K. C., Yang, T. S., Yeh, C. Y., You, J. F., Hung, H. Y., Chen, S. J., & Chen, H. C. (2015). CBB1003, a lysine-specific demethylase 1 inhibitor, suppresses colorectal cancer cells growth through down-regulation of leucine-rich repeat-containing G-protein-coupled receptor 5 expression. *J Cancer Res Clin Oncol*, *141*(1), 11-21. https://doi.org/10.1007/s00432-014-1782-4

Huang, J., Sengupta, R., Espejo, A. B., Lee, M. G., Dorsey, J. A., Richter, M., Opravil, S., Shiekhattar, R., Bedford, M. T., Jenuwein, T., & Berger, S. L. (2007). p53 is regulated by the lysine demethylase LSD1. *Nature*, *449*(7158), 105-108. https://doi.org/10.1038/nature06092

Hyun, K., Jeon, J., Park, K., & Kim, J. (2017). Writing, erasing and reading histone lysine methylations. *Experimental & Molecular Medicine*, *49*(4), e324-e324. https://doi.org/10.1038/emm.2017.11

Im, K., Mareninov, S., Diaz, M. F. P., & Yong, W. H. (2019). An Introduction to Performing Immunofluorescence Staining. *Methods Mol Biol*, *1897*, 299-311. https://doi.org/10.1007/978-1-4939-8935-5_26

Ismail, T., Lee, H. K., Kim, C., Kwon, T., Park, T. J., & Lee, H. S. (2018). KDM1A microenvironment, its oncogenic potential, and therapeutic significance. *Epigenetics Chromatin*, *11*(1), 33. https://doi.org/10.1186/s13072-018-0203-3

Jenuwein, T., & Allis, C. D. (2001). Translating the Histone Code. *Science*, *293*(5532), 1074-1080. https://doi.org/10.1126/science.1063127

Jie, D., Zhongmin, Z., Guoqing, L., Sheng, L., Yi, Z., Jing, W., & Liang, Z. (2013). Positive expression of LSD1 and negative expression of E-cadherin correlate with metastasis and poor prognosis of colon cancer. *Dig Dis Sci*, *58*(6), 1581-1589. https://doi.org/10.1007/s10620-012-2552-2

Jin, B., Li, Y., & Robertson, K. D. (2011). DNA Methylation: Superior or Subordinate in the Epigenetic Hierarchy? *Genes & Cancer*, *2*(6), 607-617. https://doi.org/10.1177/1947601910393957

Kang, E., Yousefi, M., & Gruenheid, S. (2016). R-Spondins Are Expressed by the Intestinal Stroma and are Differentially Regulated during Citrobacter rodentium- and DSS-Induced Colitis in Mice. *PLoS One*, *11*(4), e0152859. https://doi.org/10.1371/journal.pone.0152859

Karakaidos, P., Verigos, J., & Magklara, A. (2019). LSD1/KDM1A, a Gate-Keeper of Cancer Stemness and a Promising Therapeutic Target. *Cancers (Basel)*, *11*(12). https://doi.org/10.3390/cancers11121821

Kim, K.-A., Zhao, J., Andarmani, S., Kakitani, M., Oshima, T., Binnerts, M. E., Abo, A., Tomizuka, K., & Funk, W. D. (2006). R-Spondin Proteins: A Novel Link to β-catenin Activation. *Cell Cycle*, *5*(1), 23-26. https://doi.org/10.4161/cc.5.1.2305

Kim, S. W., Roh, J., & Park, C. S. (2016). Immunohistochemistry for Pathologists: Protocols, Pitfalls, and Tips. *J Pathol Transl Med*, *50*(6), 411-418. https://doi.org/10.4132/jptm.2016.08.08

Koo, B. K., & Clevers, H. (2014). Stem cells marked by the R-spondin receptor LGR5. *Gastroenterology*, *147*(2), 289-302. https://doi.org/10.1053/j.gastro.2014.05.007

Korinek, V., Barker, N., Moerer, P., Van Donselaar, E., Huls, G., Peters, P. J., & Clevers, H. (1998). Depletion of epithelial stem-cell compartments in the small intestine of mice lacking Tcf-4. *Nat Genet*, *19*(4), 379-383. https://doi.org/10.1038/1270

Kosinski, C., Li, V. S. W., Chan, A. S. Y., Zhang, J., Ho, C., Tsui, W. Y., Chan, T. L., Mifflin, R. C., Powell, D. W., Yuen, S. T., Leung, S. Y., & Chen, X. (2007). Gene expression patterns of human colon tops and basal crypts and BMP antagonists as intestinal stem cell niche factors. *Proceedings of the National Academy of Sciences*, *104*(39), 15418-15423. https://doi.org/10.1073/pnas.0707210104

Kuhnert, F., Davis, C. R., Wang, H. T., Chu, P., Lee, M., Yuan, J., Nusse, R., & Kuo, C. J. (2004). Essential requirement for Wnt signaling in proliferation of adult small intestine and colon revealed by adenoviral expression of Dickkopf-1. *Proceedings of the National Academy of Sciences*, *101*(1), 266-271. https://doi.org/10.1073/pnas.2536800100

Langlands, A. J., Carroll, T. D., Chen, Y., & Näthke, I. (2018). Chir99021 and Valproic acid reduce the proliferative advantage of Apc mutant cells. *Cell Death Dis*, *9*(3), 255. https://doi.org/10.1038/s41419-017-0199-9

Lei, N. Y., Jabaji, Z., Wang, J., Joshi, V. S., Brinkley, G. J., Khalil, H., Wang, F., Jaroszewicz, A., Pellegrini, M., Li, L., Lewis, M., Stelzner, M., Dunn, J. C. Y., & Martín, M. G. (2014). Intestinal Subepithelial Myofibroblasts Support the Growth of Intestinal Epithelial Stem Cells. *PLoS One*, *9*(1), e84651. https://doi.org/10.1371/journal.pone.0084651

Leong, T. Y., & Leong, A. S. (2007). How does antigen retrieval work? *Adv Anat Pathol*, *14*(2), 129-131. https://doi.org/10.1097/PAP.0b013e31803250c7

Li-Cor. (2017). Tissue Section Imaging. https://www.licor.com/bio/support/

Lin, Y., Wu, Y., Li, J., Dong, C., Ye, X., Chi, Y. I., Evers, B. M., & Zhou, B. P. (2010). The SNAG domain of Snail1 functions as a molecular hook for recruiting lysine-specific demethylase 1. *Embo j*, *29*(11), 1803-1816. https://doi.org/10.1038/emboj.2010.63

Lindholm, H. T., Parmar, N., Drurey, C., Ostrop, J., Díez-Sanchez, A., Maizels, R. M., & Oudhoff, M. J. (2020). Developmental pathways regulate cytokine-driven effector and feedback responses in the intestinal epithelium. *bioRxiv*, 2020.2006.2019.160747. https://doi.org/10.1101/2020.06.19.160747

Lv, T., Yuan, D., Miao, X., Lv, Y., Zhan, P., Shen, X., & Song, Y. (2012). Over-Expression of LSD1 Promotes Proliferation, Migration and Invasion in Non-Small Cell Lung Cancer. *PLoS One*, *7*(4), e35065. https://doi.org/10.1371/journal.pone.0035065

Mahmood, T., & Yang, P. C. (2012). Western blot: technique, theory, and trouble shooting. *N Am J Med Sci*, *4*(9), 429-434. https://doi.org/10.4103/1947-2714.100998

Mallo, G. V., Rechreche, H., Frigerio, J. M., Rocha, D., Zweibaum, A., Lacasa, M., Jordan, B. R., Dusetti, N. J., Dagorn, J. C., & Iovanna, J. L. (1997). Molecular cloning, sequencing and expression of the mRNA encoding human Cdx1 and Cdx2 homeobox. Down-regulation of Cdx1 and Cdx2 mRNA expression during colorectal carcinogenesis. *Int J Cancer*, *74*(1), 35-44. https://doi.org/10.1002/(sici)1097-0215(19970220)74:1<35::aid-ijc7>3.0.co;2-1

Marabelli, C., Marrocco, B., & Mattevi, A. (2016). The growing structural and functional complexity of the LSD1/KDM1A histone demethylase. *Current Opinion in Structural Biology*, *41*, 135-144. https://doi.org/10.1016/j.sbi.2016.07.011

Marshman, E., Booth, C., & Potten, C. S. (2002). The intestinal epithelial stem cell. *Bioessays*, *24*(1), 91-98. https://doi.org/10.1002/bies.10028

Montgomery, R. K., Carlone, D. L., Richmond, C. A., Farilla, L., Kranendonk, M. E. G., Henderson, D. E., Baffour-Awuah, N. Y., Ambruzs, D. M., Fogli, L. K., Algra, S., & Breault, D. T. (2011). Mouse telomerase reverse transcriptase (mTert) expression marks slowly cycling intestinal stem cells. *Proceedings of the National Academy of Sciences*, *108*(1), 179-184. https://doi.org/10.1073/pnas.1013004108

Moolenbeek, C., & Ruitenberg, E. J. (1981). The "Swiss roll": a simple technique for histological studies of the rodent intestine. *Lab Anim*, *15*(1), 57-59. https://doi.org/10.1258/002367781780958577

Moser, A. R., Luongo, C., Gould, K. A., McNeley, M. K., Shoemaker, A. R., & Dove, W. F. (1995). ApcMin: A mouse model for intestinal and mammary tumorigenesis. *European Journal of Cancer*, *31*(7-8), 1061-1064. https://doi.org/10.1016/0959-8049(95)00181-h

Muñoz, J., Stange, D. E., Schepers, A. G., Van De Wetering, M., Koo, B.-K., Itzkovitz, S., Volckmann, R., Kung, K. S., Koster, J., Radulescu, S., Myant, K., Versteeg, R., Sansom, O. J., Van Es, J. H., Barker, N., Van Oudenaarden, A., Mohammed, S., Heck, A. J. R., & Clevers, H. (2012). The Lgr5 intestinal stem cell signature: robust expression of proposed quiescent '+4' cell markers. *The EMBO Journal*, *31*(14), 3079-3091. https://doi.org/10.1038/emboj.2012.166

Nusse, R., & Clevers, H. (2017). Wnt/β-Catenin Signaling, Disease, and Emerging Therapeutic Modalities. *Cell*, *169*(6), 985-999. https://doi.org/10.1016/j.cell.2017.05.016

Parmar, N., Burrows, K., Vornewald, P. M., Lindholm, H. T., Zwiggelaar, R. T., Díez-Sánchez, A., Martín-Alonso, M., Fosslie, M., Vallance, B. A., Dahl, J. A., Zaph, C., & Oudhoff, M. J. (2021). Intestinal-epithelial LSD1 controls goblet cell maturation and effector responses required for gut immunity to bacterial and helminth infection. *PLOS Pathogens*, *17*(3), e1009476. https://doi.org/10.1371/journal.ppat.1009476

Parmar, N., Burrows, K., Vornewald, P. M., Lindholm, H. T., Zwiggelaar, R. T., Díez-Sánchez, A., Martín-Alonso, M., Fosslie, M., Vallance, B. A., Dahl, J. A., Zaph, C., & Oudhoff, M. J. (2021). Intestinal-epithelial LSD1 controls goblet cell maturation and effector responses required for gut immunity to bacterial and helminth infection. *PLoS Pathog*, *17*(3), e1009476. https://doi.org/10.1371/journal.ppat.1009476

Polychronopoulos, P., Magiatis, P., Skaltsounis, A. L., Myrianthopoulos, V., Mikros, E., Tarricone, A., Musacchio, A., Roe, S. M., Pearl, L., Leost, M., Greengard, P., & Meijer, L. (2004). Structural basis for the synthesis of indirubins as potent and

selective inhibitors of glycogen synthase kinase-3 and cyclin-dependent kinases. *J Med Chem*, *47*(4), 935-946. https://doi.org/10.1021/jm031016d

Potten, C. S. (1977). Extreme sensitivity of some intestinal crypt cells to X and gamma irradiation. *Nature*, *269*(5628), 518-521. https://doi.org/10.1038/269518a0

Rodríguez-Colman, M. J., Schewe, M., Meerlo, M., Stigter, E., Gerrits, J., Pras-Raves, M., Sacchetti, A., Hornsveld, M., Oost, K. C., Snippert, H. J., Verhoeven-Duif, N., Fodde, R., & Burgering, B. M. T. (2017). Interplay between metabolic identities in the intestinal crypt supports stem cell function. *Nature*, *543*(7645), 424-427. https://doi.org/10.1038/nature21673

Rubinfeld, B., Souza, B., Albert, I., Munemitsu, S., & Polakis, P. (1995). The APC protein and E-cadherin form similar but independent complexes with alpha-catenin, beta-catenin, and plakoglobin. *J Biol Chem*, *270*(10), 5549-5555. https://doi.org/10.1074/jbc.270.10.5549

Salon, C., Lantuejoul, S., Eymin, B., Gazzeri, S., Brambilla, C., & Brambilla, E. (2005). The E-cadherin-beta-catenin complex and its implication in lung cancer progression and prognosis. *Future Oncol*, *1*(5), 649-660. https://doi.org/10.2217/14796694.1.5.649

Sancho, R., Cremona, C. A., & Behrens, A. (2015). Stem cell and progenitor fate in the mammalian intestine: Notch and lateral inhibition in homeostasis and disease. *EMBO Rep*, *16*(5), 571-581. https://doi.org/10.15252/embr.201540188

Sangiorgi, E., & Capecchi, M. R. (2008). Bmi1 is expressed in vivo in intestinal stem cells. *Nat Genet*, *40*(7), 915-920. https://doi.org/10.1038/ng.165

Sasaki, N., Sachs, N., Wiebrands, K., Ellenbroek, S. I. J., Fumagalli, A., Lyubimova, A., Begthel, H., Van Den Born, M., Van Es, J. H., Karthaus, W. R., Li, V. S. W., López-Iglesias, C., Peters, P. J., Van Rheenen, J., Van Oudenaarden, A., & Clevers, H. (2016). Reg4+ deep crypt secretory cells function as epithelial niche for Lgr5+ stem cells in colon. *Proceedings of the National Academy of Sciences*, *113*(37), E5399-E5407. https://doi.org/10.1073/pnas.1607327113

Sato, N., Meijer, L., Skaltsounis, L., Greengard, P., & Brivanlou, A. H. (2004). Maintenance of pluripotency in human and mouse embryonic stem cells through activation of Wnt signaling by a pharmacological GSK-3-specific inhibitor. *Nat Med*, *10*(1), 55-63. https://doi.org/10.1038/nm979

Sato, T., & Clevers, H. (2013). Growing self-organizing mini-guts from a single intestinal stem cell: mechanism and applications. *Science*, *340*(6137), 1190-1194. https://doi.org/10.1126/science.1234852

Sato, T., Stange, D. E., Ferrante, M., Vries, R. G., Van Es, J. H., Van den Brink, S., Van Houdt, W. J., Pronk, A., Van Gorp, J., Siersema, P. D., & Clevers, H. (2011). Long-term expansion of epithelial organoids from human colon, adenoma, adenocarcinoma, and Barrett's epithelium. *Gastroenterology*, *141*(5), 1762-1772. https://doi.org/10.1053/j.gastro.2011.07.050

Sato, T., van Es, J. H., Snippert, H. J., Stange, D. E., Vries, R. G., van den Born, M., Barker, N., Shroyer, N. F., van de Wetering, M., & Clevers, H. (2011). Paneth cells constitute the niche for Lgr5 stem cells in intestinal crypts. *Nature*, *469*(7330), 415-418. https://doi.org/10.1038/nature09637

Sato, T., Vries, R. G., Snippert, H. J., van de Wetering, M., Barker, N., Stange, D. E., van Es, J. H., Abo, A., Kujala, P., Peters, P. J., & Clevers, H. (2009). Single Lgr5 stem cells build crypt-villus structures in vitro without a mesenchymal niche. *Nature*, *459*(7244), 262-265. https://doi.org/10.1038/nature07935

Schneider, C. A., Rasband, W. S., & Eliceiri, K. W. (2012). NIH Image to ImageJ: 25 years of image analysis. *Nature Methods*, *9*(7), 671-675. https://doi.org/10.1038/nmeth.2089

Schutz Geschwender, A. (2012). Near-Infrared Fluorescent Methods for Protein Analysis. *4*, 56-59.

Smith, P. K., Krohn, R. I., Hermanson, G. T., Mallia, A. K., Gartner, F. H., Provenzano, M. D., Fujimoto, E. K., Goeke, N. M., Olson, B. J., & Klenk, D. C. (1985). Measurement of protein using bicinchoninic acid. *Anal Biochem*, *150*(1), 76-85. https://doi.org/10.1016/0003-2697(85)90442-7

Takeda, N., Jain, R., Leboeuf, M. R., Wang, Q., Lu, M. M., & Epstein, J. A. (2011). Interconversion Between Intestinal Stem Cell Populations in Distinct Niches. *Science*, *334*(6061), 1420-1424. https://doi.org/10.1126/science.1213214

Takeichi, M. (1990). CADHERINS: A MOLECULAR FAMILY IMPORTANT IN SELECTIVE CELL-CELL ADHESION. *Annual Review of Biochemistry*, *59*(1), 237-252. https://doi.org/10.1146/annurev.bi.59.070190.001321

Thermo-Fisher. (2017). Protein assay technical handbook. In T. F. Scientific (Ed.), *https://assets.thermofisher.com/TFS-Assets/LSG/brochures/protein-assay-technical-handook.pdf?icid=linchpin15-protein-assay-technical-handook*.

Thorn, K. (2016). A quick guide to light microscopy in cell biology. *Mol Biol Cell*, *27*(2), 219-222. https://doi.org/10.1091/mbc.E15-02-0088

van der Flier, L. G., Haegebarth, A., Stange, D. E., van de Wetering, M., & Clevers, H. (2009). OLFM4 is a robust marker for stem cells in human intestine and marks a subset of colorectal cancer cells. *Gastroenterology*, *137*(1), 15-17. https://doi.org/10.1053/j.gastro.2009.05.035

Van Es, J. H., Haegebarth, A., Kujala, P., Itzkovitz, S., Koo, B. K., Boj, S. F., Korving, J., Van Den Born, M., Van Oudenaarden, A., Robine, S., & Clevers, H. (2012). A Critical Role for the Wnt Effector Tcf4 in Adult Intestinal Homeostatic Self-Renewal. *Mol Cell Biol*, *32*(10), 1918-1927. https://doi.org/10.1128/mcb.06288-11

Velcich, A., Yang, W., Heyer, J., Fragale, A., Nicholas, C., Viani, S., Kucherlapati, R., Lipkin, M., Yang, K., & Augenlicht, L. (2002). Colorectal cancer in mice genetically deficient in the mucin Muc2. *Science*, *295*(5560), 1726-1729. https://doi.org/10.1126/science.1069094

Wallach, T. E., & Bayrer, J. R. (2017). Intestinal Organoids: New Frontiers in the Study of Intestinal Disease and Physiology. *J Pediatr Gastroenterol Nutr*, *64*(2), 180-185. https://doi.org/10.1097/mpg.0000000000001411

Wang, F., Scoville, D., He, X. C., Mahe, M. M., Box, A., Perry, J. M., Smith, N. R., Lei, N. Y., Davies, P. S., Fuller, M. K., Haug, J. S., McClain, M., Gracz, A. D., Ding, S., Stelzner, M., Dunn, J. C. Y., Magness, S. T., Wong, M. H., Martin, M. G., . . . Li, L. (2013). Isolation and Characterization of Intestinal Stem Cells Based on Surface Marker Combinations and Colony-Formation Assay. *Gastroenterology*, *145*(2), 383-395.e321. https://doi.org/10.1053/j.gastro.2013.04.050

Wang, Y., Poulin, E. J., & Coffey, R. J. (2013). LRIG1 is a triple threat: ERBB negative regulator, intestinal stem cell marker and tumour suppressor. *British Journal of Cancer*, *108*(9), 1765-1770. https://doi.org/10.1038/bjc.2013.138

Wijnhoven, B. P. L., Dinjens, W. N. M., & Pignatelli, M. (2002). E-cadherin—catenin cell—cell adhesion complex and human cancer. *British Journal of Surgery*, *87*(8), 992-1005. https://doi.org/10.1046/j.1365-2168.2000.01513.x

Wong, V. W. Y., Stange, D. E., Page, M. E., Buczacki, S., Wabik, A., Itami, S., Van De Wetering, M., Poulsom, R., Wright, N. A., Trotter, M. W. B., Watt, F. M., Winton, D. J., Clevers, H., & Jensen, K. B. (2012). Lrig1 controls intestinal stem-cell homeostasis by negative regulation of ErbB signalling. *Nat Cell Biol*, *14*(4), 401-408. https://doi.org/10.1038/ncb2464

Yan, K. S., Chia, L. A., Li, X., Ootani, A., Su, J., Lee, J. Y., Su, N., Luo, Y., Heilshorn, S. C., Amieva, M. R., Sangiorgi, E., Capecchi, M. R., & Kuo, C. J. (2012). The intestinal stem cell markers Bmi1 and Lgr5 identify two functionally distinct populations. *Proc Natl Acad Sci U S A*, *109*(2), 466-471. https://doi.org/10.1073/pnas.1118857109

Zhao, M., Mishra, L., & Deng, C.-X. (2018). The role of TGF-β/SMAD4 signaling in cancer. *International Journal of Biological Sciences*, *14*(2), 111-123. https://doi.org/10.7150/ijbs.23230

Zwiggelaar, R. T., Lindholm, H. T., Fosslie, M., Terndrup Pedersen, M., Ohta, Y., Díez-Sánchez, A., Martín-Alonso, M., Ostrop, J., Matano, M., Parmar, N., Kvaløy, E., Spanjers, R. R., Nazmi, K., Rye, M., Drabløs, F., Arrowsmith, C., Arne Dahl, J., Jensen, K. B., Sato, T., & Oudhoff, M. J. (2020). LSD1 represses a neonatal/reparative gene program in adult intestinal epithelium. *Science Advances*, *6*(37), eabc0367. https://doi.org/10.1126/sciadv.abc0367